J. Appl. Comput. Mech., xx(x) (2021) 1-19
DOI: 10.22055/JACM.2021.38131.3159

ISSN: 2383-4536
jacm.scu.ac.ir

Shahid Chamran University of Ahvaz

Journal of Applied and Computational Mechanics

Research Paper

# Size Effect on the Axisymmetric Vibrational Response of Functionally Graded Circular Nano-Plate Based on the Nonlocal Stress-Driven Method

**Mojtaba Shariati[1], Mohammad Shishehsaz[2], Reza Mosalmani[3], S. Alireza S. Roknizadeh[4]**

[1] Department of Mechanical Engineering, Shahid Chamran University of Ahvaz, Ahvaz, Iran, Email: mojtaba.shariati456@gmail.com

[2] Department of Mechanical Engineering, Shahid Chamran University of Ahvaz, Ahvaz, Iran, Email: mshishehsaz@scu.ac.ir

[3] Department of Mechanical Engineering, Shahid Chamran University of Ahvaz, Ahvaz, Iran, Email: mosalmani@scu.ac.ir

[4] Department of Mechanical Engineering, Shahid Chamran University of Ahvaz, Ahvaz, Iran, Email: s.roknizadeh@scu.ac.ir

Received August 01 2021; Revised September 20 2021; Accepted for publication September 21 2021.
Corresponding author: M. Shishehsaz (mshishehsaz@scu.ac.ir)


**Abstract.** In this work, the axisymmetric-vibrational behavior of a size-dependent circular nano-plate with functionally graded material with different types of boundary conditions was investigated. The analysis was performed based on the Stress-driven model (SDM) and Strain-gradient theory (SGT) in conjunction with classical plate theory. The governing equations of motion and their corresponding equations for boundary conditions were obtained based on Hamilton's principle and solved using the generalized differential quadrature rule. Results show that this method is applicable to the vibrational analysis of such structures with a fast convergence rate; as $N$ approaches 6 for the first mode, and 10 for the second as well as the third and fourth modes, regardless of the type of boundary condition. In both models, the influences of various parameters such as size-effect parameter $L_c$, material heterogeneity index $n$, and types of boundary conditions were obtained on the first four modes and compared with each other. Results indicate that the natural frequencies in these modes increase with an increase in the heterogeneity index $n$, and size-effect parameter $L_c$. Additionally, these parameters appear to have a stiffening effect on the nano-plate vibrational behavior. However, for a nano-plate resting on a knife or simply supported edge, in the first mode, the SDM shows a more stiffening effect on the plate behavior as compared with the SGT. Nonetheless, for the clamped and free edge boundary conditions, both models predicted the same behavior. The SGT showed a higher-stiffening effect only in the fourth mode, for all types of considered boundary conditions.

**Keywords:** Vibrational response, functionally graded material, circular nano-plate, stress-driven model, strain gradient theory.

## 1. Introduction

Humans are always looking for better ways to live. One of the newest solutions to reach this goal is the use of nano-technology. Due to the severe need for high technology in engineering and medical sciences, there is a special focus on the development of nano-science, as well as the introduction of proper models for the prediction of their behaviors (i.e., the development of special tools and drugs for special applications). Nanomedicine and nano-delivery systems show a bright horizon for treating incurable diseases. Another important application of nano-drugs and nanostructures is in the timely detection of diseases. Engineers have played an important and undeniable role in this regard. Many diagnostic devices and effective drugs in the treatment process are designed and built by engineers. Drugs made using nano-technology are so precise that their side effects are very low for patients.

It is now well known that the behavior of materials at the nano-scale is quite different from those at the macro-scale level, if not being contradictory. Therefore, scientists cannot study nano-structures based on the usual theories available on macro-scale materials. To this end, a few non-classical theories capable of studying nano-materials and nanostructures have been proposed and developed. Among these theories, one can point out the nonlocal elasticity theory [1], strain gradient theory [2-4], surface effect elasticity, couple stress theory, and stress-driven model [5-9].

When the feature size of a structure is reduced to the nano-scale, classical mechanics will break down firstly at the thickness dimensions due to the simple fact that the plate's thickness dimension is far smaller than its length dimension, as illustratively shown in [10]. This in turn implies that the thickness effect is likely to play a dominant role in the contribution of size dependence. This fact has been also pointed out by molecular dynamics simulations [11]. Jiang *et al.* [12] investigated the elastic buckling of Euler-Bernoulli and Timoshenko beams under different boundary conditions using the stress-driven model. Barretta *et al.* [13] studied the buckling behavior of Bernoulli-Euler size-dependent beams by a stress-driven model. Free flexural vibrations of nano-beams were studied using a stress-driven model and Euler-Bernoulli kinematics by Luciano *et al.* [14]. Pinnola *et al.* [15] described the random

Published online: September 24 2021

vibration behavior of Bernoulli–Euler nano-beams with external damping in the frameworks of the stress-driven model. Bending and buckling of Timoshenko nano-beams were studied by Luciano *et al.* [16] using a non-local stress-driven model. He *et al.* [17] utilized the stress-driven model to study the free vibration of Euler–Bernoulli and Timoshenko size-dependent beams. The bending behavior of Timoshenko nano-beams made of functionally graded materials was analyzed by Roghani and Rouhi [18] in the frameworks of integral (original) formulation of Eringen's nonlocal theory. Romano and Barretta [19] proposed an integral type nonlocal elasticity model for the bending of small-scale beams. Apuzzo *et al.* [20] studied the free vibration behavior of small-scale beams using an integral form of nonlocal theory. Other researchers have also studied nano-mechanics and nanostructures utilizing other nonlocal models [21-45].

Zarei *et. al* [46] studied the vibrational and buckling properties of circular nano-plate with variable thickness and in-plane forces. Linear thickness variation in the radial direction and the nonlocal elasticity theory were used to model the size-dependent effects. Additionally, differential transform and Raleigh-Ritz methods were used to obtain the frequency equations for the clamped and simply supported boundary conditions. In this article, the effect of mode number, nonlocal, and taper parameters on the natural frequency were investigated. Results showed that increasing the taper parameter causes an increase in buckling load and natural frequencies. Using the stress-driven model and Kirchhoff plate theory, R. Barretta *et. al* [47] studied the behavior of an axisymmetric circular/ annular nano-plate and compared the results with those of the strain gradient model of elasticity generated by Reissner's variational principle. Shishesaz *et. al* [48] studied the small-scale effect on the linear free-field vibration of a nano-circular plate using classical plate theory, nonlocal elasticity theory, and the Adomian decomposition method. The first five axisymmetric natural frequencies and displacements of the nano-circular plate were obtained and numerical results were deduced to illustrate the influence of nonlocal parameters on the natural frequencies and displacements of the structure in question. Shariati *et. al* [49] investigated the nonlinear free vibration of a circular nano-plate considering small scale effects by using the nonlocal elasticity theory and variational iteration method. Li *et. al* [50] proposed a size-dependent nonlinear theory for the bending behavior of an axisymmetric thin circular plate. They used the Zhou strain gradient theory, the von Kármán geometric nonlinearity, and the principle of minimum potential energy to analyze the nonlinear axisymmetric bending of the plate. Al-Furjan *et. al* [51] studied the vibrational behavior of a viscoelastic composite annular micro-plate resting on a viscoelastic foundation based on the Kelvin-Voight model and the modified couple stress theory. The effects of the length scale parameter, radius ratio, circumferential and radial mode numbers, geometry of the laminated layer, and boundary conditions were studied on the frequency responses of the annular microplate, based on the generalized differential quadrature method (GDQM), for various boundary conditions.

On the other hand, micro-structures with functionally graded materials (FGMs), in which the properties vary from one material to another across the thickness, are not prone to be adequately modeled by employing the classical continuum mechanics alone. However, using the non-classical continuum mechanics, with spatial variations in material properties, will produce more accurate results, especially in vibrational problems [42, 52]. In such cases, it is also possible to allow for variations of elastic properties in t he plate platform, as considered in [53, 54]. The transverse free vibrational behavior of an axisymmetric functionally graded circular nano-plate with radial loads was studied by Luo *et. al* [55]. They used the nonlocal strain gradient approach and Mindlin plate theory to model the problem and solved the equation of motion using the differential quadrature method. They showed that the natural frequencies of the circular nanoplates decrease with an increase in the radial compressive load while increase with the increase in the radial tensile load. They also showed that the first-mode natural frequency reduces to zero under a certain radial compressive load, resulting in dynamic instability. Pourabdy *et. al* [56], studied the linear vibrational behavior of functionally graded circular nano-plates based on the integral form of the nonlocal strain gradient theory, generalized differential quadrature rule, and Galerkin weighted residual method. The dynamic behavior of the structure in question was studied under different types of boundary conditions. Free vibration behavior of functionally graded nano-beam was investigated by Barretta *et al.* [57] based on strain gradient theory and stress-driven model. Zhang and Qing [58] employed a stress-driven model to study the buckling behavior of functionally graded curved sandwich microbeams. Penna *et al.* [59] utilized a stress-driven model to study the nonlinear free vibrations analysis of geometrically imperfect Bernoulli-Euler functionally graded nano-beams subjected to different boundary conditions.

A comprehensive survey of the literature reveals that there is a lack of published data on the nano-plate vibrational behavior, based on the stress-driven model. So far, most of the studies performed by other researchers have focused on the vibrational behavior of beam structures. Therefore, the authors have tried to focus on the linear vibrational behavior of a functionally graded circular nano-plate using the stress-driven model, based on four types of commonly used clamped, simply supported, free, and knife-edge boundary conditions. The method used in this research can overcome any pitfalls that can exist in the dynamic behavior of circular nano-plate under different types of boundary conditions if other nonlocal theories are used instead. Additionally, the results of this work can initiate a set point for the study of vibrational behavior of the circular nano-plates, using SDM. In this study, the process of applying different theories (models) to achieve the governing equations and their solutions are well described in subsequent sections 2 and 3. The generalized differential quadrature rule (GDQR) is used to find a solution. Validation of the solution procedure and its corresponding results is discussed in section 4.

## 2. Problem Formulation, Equation of Motion Based on Stress Resultants

A circular nano-plate of thickness $h$ and radius $R$ is shown in Fig. 1. To study the vibrational behavior of this plate, the strain-driven nonlocal integral elasticity model (SDM) is used in conjunction with the classical plate theory (CLPT). The equilibrium equations are deduced using an axisymmetric cylindrical coordinate system ($r$, $z$).

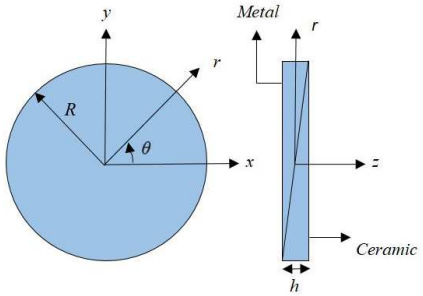


**Fig. 1.** Coordinate system and configuration of the nano-plate.

As mentioned in the "Introduction" section, generally a functionally graded material, FGM, has varying material properties. For simplicity, the selected FGM material used for the nano-plate is composed of two *isotropic materials*, namely, ceramic and metal. In this case, the material properties, namely Young's modulus *E*, and mass density $\rho$ are assumed to vary across the thickness according to Eq. (1), while for simplicity the Poisson's ratio $\nu$ is assumed to be constant in the thickness direction.

$$E(r,z,t)=E_c V^n+E_m\left(1-V^n\right)\ ,\ \rho(r,z,t)=\rho_c V^n+\rho_m\left(1-V^n\right)\ ,\ \nu(r,z,t)=\nu. \tag{1}$$

The subscripts *m* and *c* refer to the metal and ceramic constituents, respectively; *n* is the gradient index, and *V* is the volume fraction of the ceramic material, that is assumed to follow the power-law distribution as:

$$V=\frac{2z+h}{2h}\quad ,\quad -\frac{h}{2}\le z\le+\frac{h}{2} \tag{2}$$

Based on the Kirchhoff assumption for the thin plates, the shear deformation and rotary inertia can be omitted. Moreover, the component of displacement field in the radial *r*-direction $u_r$ and the transverse z-direction $u_z$ are assumed to vary as follows [60];

$$u_r(r,z,t)=u_0(r,t)-z\frac{\partial w_0}{\partial r}(r,t)\quad ,\quad u_z(r,z,t)=w_0(r,t) \tag{3}$$

where $u_0$ and $w_0$ are the displacement components of the mid-plane surface in the radial and transverse directions, respectively. On the other hand, based on the strain-displacement relationships, the non-zero strain components are given by [60];

$$\varepsilon_{rr}=\frac{\partial u_r}{\partial r}=\frac{\partial u_0}{\partial r}-z\frac{\partial^2 w_0}{\partial r^2}=\varepsilon_{rr}^0+z\kappa_{rr}\quad ,\quad \varepsilon_{\theta\theta}=\frac{u_r}{r}=\frac{u_0}{r}-z\frac{1}{r}\frac{\partial w_0}{\partial r}=\varepsilon_{\theta\theta}^0+z\kappa_{\theta\theta}. \tag{4}$$

where $\varepsilon_{rr}^0$ and $\varepsilon_{\theta\theta}^0$ are the normal radial and hoop local elastic strains associated with the mid-plane surface and $\kappa_{rr}$ and $\kappa_{\theta\theta}$ are the principal curvatures of the deflected surface.
Using Hamilton's principle, the differential equations of motion and boundary conditions, based on Kirchhoff's plate model, are expressed as [60]:

$$\begin{cases}\dfrac{1}{r}\left\{\dfrac{\partial}{\partial r}(rN_{rr})-N_{\theta\theta}\right\}=I_0\dfrac{\partial^2 u_0}{\partial t^2}-I_1\dfrac{\partial^2}{\partial t^2}\dfrac{\partial w_0}{\partial r}\\ \dfrac{1}{r}\left\{\dfrac{\partial^2}{\partial r^2}(rM_{rr})-\dfrac{\partial M_{\theta\theta}}{\partial r}\right\}=I_0\dfrac{\partial^2 w_0}{\partial t^2}+I_1\dfrac{\partial^2}{\partial t^2}\left(\dfrac{1}{r}\dfrac{\partial}{\partial r}(ru_0)\right)-I_2\dfrac{\partial^2}{\partial t^2}\left(\dfrac{1}{r}\dfrac{\partial}{\partial r}\left(r\dfrac{\partial w_0}{\partial r}\right)\right)\end{cases} \tag{5-a}$$

$$N_{rr}=0\ \text{ or }\ u_0=0\quad ,\quad Q_r=\frac{1}{r}\left(\frac{\partial}{\partial r}(rM_{rr})-M_{\theta\theta}\right)=0\ \text{ or }\ w_0=0\quad ,\quad M_{rr}=0\ \text{ or }\ \frac{\partial w_0}{\partial r}=0. \tag{5-b}$$

where, $Q_r$ is the transverse shearing force, and the stress resultants $N_{rr}$, $N_{\theta\theta}$, $M_{rr}$, and $M_{\theta\theta}$, as well as the mass moments of inertias $I_0$, $I_1$, and $I_2$, are defined as:

$$(N_{rr}\ ,\ N_{\theta\theta},\ M_{rr}\ ,\ M_{\theta\theta})=\int_{-\frac{h}{2}}^{+\frac{h}{2}}(\sigma_{rr}\ ,\ \sigma_{\theta\theta},\ z\sigma_{rr}\ ,\ z\sigma_{\theta\theta})dz \tag{6-a}$$

$$(I_0,I_1,I_2)=\int_{-\frac{h}{2}}^{+\frac{h}{2}}\left(1,z,z^2\right)\rho dz \tag{6-b}$$

### 2.1. Equations of motion based on stress-driven model (SDM)

Based on the classical plate theory, the strain components are written in terms of stress components as:

$$\varepsilon_{rr}=\frac{1}{E}(\sigma_{rr}-\nu\sigma_{\theta\theta})\quad ,\quad \varepsilon_{\theta\theta}=\frac{1}{E}(-\nu\sigma_{rr}+\sigma_{\theta\theta}). \tag{7}$$

Using Eq. (4), (6-a), and (7) one can obtain:

$$\begin{bmatrix}A&0&B&0\\B&0&D&0\\0&A&0&B\\0&B&0&D\end{bmatrix}\begin{Bmatrix}\varepsilon_{rr}^0\\\varepsilon_{\theta\theta}^0\\\kappa_{rr}\\\kappa_{\theta\theta}\end{Bmatrix}=\begin{bmatrix}1&-\nu&0&0\\0&0&1&-\nu\\-\nu&1&0&0\\0&0&-\nu&1\end{bmatrix}\begin{Bmatrix}N_{rr}\\N_{\theta\theta}\\M_{rr}\\M_{\theta\theta}\end{Bmatrix} \tag{8-a}$$

where the parameters (*A*, *B*, and *D*) are the stiffness coefficients and are defined as follows:

$$(A,B,D)=\int_{-h/2}^{+h/2}E(z)\left(1,z,z^2\right)dz \tag{8-b}$$

On using Eq. (8-a), $\varepsilon_{rr}^0$ and $\kappa_{rr}$ can be obtained as:

$$\begin{Bmatrix}\varepsilon_{rr}^0\\\kappa_{rr}\end{Bmatrix}=\begin{bmatrix}A&B\\B&D\end{bmatrix}^{-1}\begin{bmatrix}1&-\nu&0&0\\0&0&1&-\nu\end{bmatrix}\begin{Bmatrix}N_{rr}\\N_{\theta\theta}\\M_{rr}\\M_{\theta\theta}\end{Bmatrix} \tag{9}$$

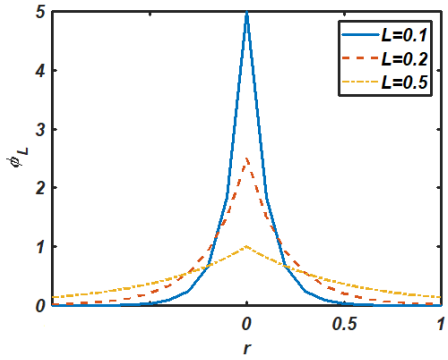


**Fig. 2.** Plot of bi-exponential kernel function, Eq. (12), for $L$=0.1, 0.2 and 0.5 [9].

The SDM proposed by Romano and Barretta for the nano-beams is used to capture the size effects in the axisymmetric nano-plat. Based on this model, assuming the non-local elasticity only for the radial strain of the mid-plane surface, $\varepsilon^0_{rr}$, and its corresponding radial curvature $\kappa_{rr}$ [61], one can write;

$$\begin{Bmatrix}\varepsilon^0_{rr}\\ \kappa_{rr}\end{Bmatrix}=\int_0^R \varphi_L \begin{bmatrix}A & B\\ B & D\end{bmatrix}^{-1}\begin{bmatrix}1 & -\nu & 0 & 0\\ 0 & 0 & 1 & -\nu\end{bmatrix}\begin{Bmatrix}N_{rr}\\ N_{\theta\theta}\\ M_{rr}\\ M_{\theta\theta}\end{Bmatrix}dr \tag{10}$$

where;

$$\varphi_L(r)=\frac{1}{2L}\exp\left(-\frac{|r|}{L}\right) \tag{11}$$

In Eq. (11), $L$ is the characteristic length that describes the size effects and $\varphi_L$ is the averaging kernel with the following properties:

$$\varphi_L(r)\geq 0 \quad , \quad \int_{-\infty}^{+\infty}\varphi_L(r)\,dr=1 \quad , \quad \lim_{L\to 0^+}\int_{-\infty}^{+\infty}\varphi_L(r-\rho)f(\rho)d\rho=f(\rho). \tag{12}$$

where $f$ is any continuous test field [61].

In this study, the type of bi-exponential kernel function used for the analysis is expressed by Eq. (12) and plotted in Fig. 2 for $L$ = 0.1, 0.2, and 0.5. One can easily prove that this function fulfils all the necessary properties given by the set of Eqs. (11).

Using this special kernel function, the nonlocal integral convolution, Eq. (10), can be reformed to the following SDM differential equation, Eq. (13-a), with the constitutive boundary conditions given in Eq. (13-b) such that:

$$\begin{Bmatrix}\varepsilon^0_{rr}-L^2\dfrac{\partial^2}{\partial r^2}\varepsilon^0_{rr}\\ \kappa_{rr}-L^2\dfrac{\partial^2}{\partial r^2}\kappa_{rr}\end{Bmatrix}=\begin{bmatrix}A & B\\ B & D\end{bmatrix}^{-1}\begin{bmatrix}1 & -\nu & 0 & 0\\ 0 & 0 & 1 & -\nu\end{bmatrix}\begin{Bmatrix}N_{rr}\\ N_{\theta\theta}\\ M_{rr}\\ M_{\theta\theta}\end{Bmatrix} \tag{13-a}$$

$$\begin{aligned}&\frac{\partial\varepsilon^0_{rr}}{\partial r}(a,t)-\frac{1}{L}\varepsilon^0_{rr}(a,t)=0 \quad , \quad \frac{\partial\varepsilon^0_{rr}}{\partial r}(b,t)+\frac{1}{L}\varepsilon^0_{rr}(b,t)=0,\\ &\frac{\partial\kappa_{rr}}{\partial r}(a,t)-\frac{1}{L}\kappa_{rr}(a,t)=0 \quad , \quad \frac{\partial\kappa_{rr}}{\partial r}(b,t)+\frac{1}{L}\kappa_{rr}(b,t)=0.\end{aligned} \tag{13-b}$$

On using Eqs. (8-b), and (13), Eq. (8-a) can be recast as Eqs. (14-a, b) such that:

$$\begin{bmatrix}1 & -\nu\\ -\nu & 1\end{bmatrix}\begin{Bmatrix}N_{rr}\\ N_{\theta\theta}\end{Bmatrix}=\begin{Bmatrix}A\left(\varepsilon^0_{rr}-L^2\dfrac{\partial^2}{\partial r^2}\varepsilon^0_{rr}\right)+B\left(\kappa_{rr}-L^2\dfrac{\partial^2}{\partial r^2}\kappa_{rr}\right)\\ A\varepsilon^0_{\theta\theta}+B\kappa_{\theta\theta}\end{Bmatrix} \tag{14-a}$$

$$\begin{bmatrix}1 & -\nu\\ -\nu & 1\end{bmatrix}\begin{Bmatrix}M_{rr}\\ M_{\theta\theta}\end{Bmatrix}=\begin{Bmatrix}B\left(\varepsilon^0_{rr}-L^2\dfrac{\partial^2}{\partial r^2}\varepsilon^0_{rr}\right)+D\left(\kappa_{rr}-L^2\dfrac{\partial^2}{\partial r^2}\kappa_{rr}\right)\\ B\varepsilon^0_{\theta\theta}+D\kappa_{\theta\theta}\end{Bmatrix} \tag{14-b}$$

Solving the Eqs. (14-a, b) gives;

$$\begin{Bmatrix}N_{rr}\\ N_{\theta\theta}\end{Bmatrix}=\frac{A}{1-\nu^2}\begin{Bmatrix}\left(\varepsilon^0_{rr}-L^2\dfrac{\partial^2}{\partial r^2}\varepsilon^0_{rr}\right)+\nu\varepsilon^0_{\theta\theta}\\ \nu\left(\varepsilon^0_{rr}-L^2\dfrac{\partial^2}{\partial r^2}\varepsilon^0_{rr}\right)+\varepsilon^0_{\theta\theta}\end{Bmatrix}+\frac{B}{1-\nu^2}\begin{Bmatrix}\left(\kappa_{rr}-L^2\dfrac{\partial^2}{\partial r^2}\kappa_{rr}\right)+\nu\kappa_{\theta\theta}\\ \nu\left(\kappa_{rr}-L^2\dfrac{\partial^2}{\partial r^2}\kappa_{rr}\right)+\kappa_{\theta\theta}\end{Bmatrix} \tag{15-a}$$

$$\begin{Bmatrix} M_{rr} \\ M_{\theta\theta} \end{Bmatrix} = \frac{B}{1-\nu^2}\begin{Bmatrix} \left(\varepsilon_{rr}^0 - L^2\frac{\partial^2}{\partial r^2}\varepsilon_{rr}^0\right) + \nu\varepsilon_{\theta\theta}^0 \\ \nu\left(\varepsilon_{rr}^0 - L^2\frac{\partial^2}{\partial r^2}\varepsilon_{rr}^0\right) + \varepsilon_{\theta\theta}^0 \end{Bmatrix} + \frac{D}{1-\nu^2}\begin{Bmatrix} \left(\kappa_{rr} - L^2\frac{\partial^2}{\partial r^2}\kappa_{rr}\right) + \nu\kappa_{\theta\theta} \\ \nu\left(\kappa_{rr} - L^2\frac{\partial^2}{\partial r^2}\kappa_{rr}\right) + \kappa_{\theta\theta} \end{Bmatrix} \tag{15-b}$$

Using Eqs. (4) and (15-a, b), the stress resultant and shear force $Q_r$ can be written in the following form:

$$\begin{aligned}
N_{rr} &= \frac{A}{1-\nu^2}\left\{\left(\frac{\partial u_0}{\partial r} - L^2\frac{\partial^3 u_0}{\partial r^3}\right) + \nu\frac{u_0}{r}\right\} - \frac{B}{1-\nu^2}\left\{\left(\frac{\partial^2 w_0}{\partial r^2} - L^2\frac{\partial^4 w_0}{\partial r^4}\right) + \nu\frac{1}{r}\frac{\partial w_0}{\partial r}\right\},\\
N_{\theta\theta} &= \frac{A}{1-\nu^2}\left\{\nu\left(\frac{\partial u_0}{\partial r} - L^2\frac{\partial^3 u_0}{\partial r^3}\right) + \frac{u_0}{r}\right\} - \frac{B}{1-\nu^2}\left\{\nu\left(\frac{\partial^2 w_0}{\partial r^2} - L^2\frac{\partial^4 w_0}{\partial r^4}\right) + \frac{1}{r}\frac{\partial w_0}{\partial r}\right\},\\
M_{rr} &= \frac{B}{1-\nu^2}\left\{\left(\frac{\partial u_0}{\partial r} - L^2\frac{\partial^3 u_0}{\partial r^3}\right) + \nu\frac{u_0}{r}\right\} - \frac{D}{1-\nu^2}\left\{\left(\frac{\partial^2 w_0}{\partial r^2} - L^2\frac{\partial^4 w_0}{\partial r^4}\right) + \nu\frac{1}{r}\frac{\partial w_0}{\partial r}\right\},\\
M_{\theta\theta} &= \frac{B}{1-\nu^2}\left\{\nu\left(\frac{\partial u_0}{\partial r} - L^2\frac{\partial^3 u_0}{\partial r^3}\right) + \frac{u_0}{r}\right\} - \frac{D}{1-\nu^2}\left\{\nu\left(\frac{\partial^2 w_0}{\partial r^2} - L^2\frac{\partial^4 w_0}{\partial r^4}\right) + \frac{1}{r}\frac{\partial w_0}{\partial r}\right\},\\
Q_r &= \frac{B}{1-\nu^2}\left(\frac{\partial^2 u_0}{\partial r^2} + \frac{1}{r}\frac{\partial u_0}{\partial r} - \frac{1}{r^2}u_0 - L^2\left(\frac{\partial^4 u_0}{\partial r^4} - \frac{\nu-1}{r}\frac{\partial^3 u_0}{\partial r^3}\right)\right)\\
&\quad - \frac{\bar{D}}{1-\nu^2}\left(\frac{\partial^3 w_0}{\partial r^3} + \frac{1}{r}\frac{\partial^2 w_0}{\partial r^2} - \frac{1}{r^2}\frac{\partial w_0}{\partial r} - L^2\left(\frac{\partial^5 w_0}{\partial r^5} - \frac{\nu-1}{r}\frac{\partial^4 w_0}{\partial r^4}\right)\right) = 0.
\end{aligned} \tag{16}$$

Additionally, substituting Eq. (16) into Eq. (5-a) gives the equations of motion for the annular nano-plate based on SDM. The resulting equations are expressed as Eqs. (17-a, b) and are written as;

$$\begin{aligned}
&\frac{1}{r}\left\{\frac{\partial}{\partial r}\left(\frac{Ar}{1-\nu^2}\left\{\left(\frac{\partial u_0}{\partial r} - L^2\frac{\partial^3 u_0}{\partial r^3}\right) + \nu\frac{u_0}{r}\right\} - \frac{Br}{1-\nu^2}\left\{\left(\frac{\partial^2 w_0}{\partial r^2} - L^2\frac{\partial^4 w_0}{\partial r^4}\right) + \nu\frac{1}{r}\frac{\partial w_0}{\partial r}\right\}\right)\right.\\
&\left. - \frac{A}{1-\nu^2}\left\{\nu\left(\frac{\partial u_0}{\partial r} - L^2\frac{\partial^3 u_0}{\partial r^3}\right) + \frac{u_0}{r}\right\} - \frac{B}{1-\nu^2}\left\{\nu\left(\frac{\partial^2 w_0}{\partial r^2} - L^2\frac{\partial^4 w_0}{\partial r^4}\right) + \frac{1}{r}\frac{\partial w_0}{\partial r}\right\}\right\} = I_0\frac{\partial^2 w_0}{\partial t^2} - I_1\frac{\partial^2}{\partial t^2}\left(\frac{\partial^2 w_0}{\partial r^2} + \frac{1}{r}\frac{\partial w_0}{\partial r}\right)
\end{aligned} \tag{17-a}$$

$$\begin{aligned}
&\frac{1}{r}\left\{\frac{\partial^2}{\partial r^2}\left(\frac{Br}{1-\nu^2}\left\{\left(\frac{\partial u_0}{\partial r} - L^2\frac{\partial^3 u_0}{\partial r^3}\right) + \nu\frac{u_0}{r}\right\} - \frac{Dr}{1-\nu^2}\left\{\left(\frac{\partial^2 w_0}{\partial r^2} - L^2\frac{\partial^4 w_0}{\partial r^4}\right) + \nu\frac{1}{r}\frac{\partial w_0}{\partial r}\right\}\right)\right.\\
&\left. - \frac{\partial}{\partial r}\left(\frac{B}{1-\nu^2}\left\{\nu\left(\frac{\partial u_0}{\partial r} - L^2\frac{\partial^3 u_0}{\partial r^3}\right) + \frac{u_0}{r}\right\} - \frac{D}{1-\nu^2}\left\{\nu\left(\frac{\partial^2 w_0}{\partial r^2} - L^2\frac{\partial^4 w_0}{\partial r^4}\right) + \frac{1}{r}\frac{\partial w_0}{\partial r}\right\}\right)\right\}\\
&= I_0\frac{\partial^2 w_0}{\partial t^2} + I_1\frac{\partial^2}{\partial t^2}\left(\frac{1}{r}\frac{\partial}{\partial r}(ru_0)\right) - I_2\frac{\partial^2}{\partial t^2}\left(\frac{1}{r}\frac{\partial}{\partial r}\left(r\frac{\partial w_0}{\partial r}\right)\right)
\end{aligned} \tag{17-b}$$

Equations (17-a, b) can be simplified into a newer form as;

$$\begin{aligned}
&\frac{A}{1-\nu^2}\left(\left\{\frac{\partial^2 u_0}{\partial r^2} + \frac{1}{r}\frac{\partial u_0}{\partial r} - \frac{1}{r^2}u_0\right\} - L^2\left\{\frac{\partial^4 u_0}{\partial r^4} - \frac{\nu-1}{r}\frac{\partial^3 u_0}{\partial r^3}\right\}\right)\\
&- \frac{B}{1-\nu^2}\left(\left\{\frac{\partial^3 w_0}{\partial r^3} + \frac{1}{r}\frac{\partial^2 w_0}{\partial r^2} - \frac{1}{r^2}\frac{\partial w_0}{\partial r}\right\} - L^2\left\{\frac{\partial^5 w_0}{\partial r^5} - \frac{\nu-1}{r}\frac{\partial^4 w_0}{\partial r^4}\right\}\right) = I_0\frac{\partial^2 u_0}{\partial t^2} - I_1\frac{\partial^2}{\partial t^2}\frac{\partial w_0}{\partial r}
\end{aligned} \tag{18-a}$$

$$\begin{aligned}
&\frac{B}{1-\nu^2}\left(\left\{\frac{\partial^3 u_0}{\partial r^3} + \frac{2}{r}\frac{\partial^2 u_0}{\partial r^2} - \frac{1}{r^2}\frac{\partial u_0}{\partial r} + \frac{1}{r^3}u_0\right\} - L^2\left\{\frac{\partial^5 u_0}{\partial r^5} - \frac{\nu-2}{r}\frac{\partial^4 u_0}{\partial r^4}\right\}\right)\\
&- \frac{D}{1-\nu^2}\left(\left\{\frac{\partial^4 w_0}{\partial r^4} + \frac{2}{r}\frac{\partial^3 w_0}{\partial r^3} - \frac{1}{r^2}\frac{\partial^2 w_0}{\partial r^2} + \frac{1}{r^3}\frac{\partial w_0}{\partial r}\right\} - L^2\left\{\frac{\partial^6 w_0}{\partial r^6} - \frac{\nu-2}{r}\frac{\partial^5 w_0}{\partial r^5}\right\}\right)\\
&= I_0\frac{\partial^2 w_0}{\partial t^2} + I_1\frac{\partial^2}{\partial t^2}\left(\frac{\partial u_0}{\partial r} + \frac{1}{r}u_0\right) - I_2\frac{\partial^2}{\partial t^2}\left(\frac{\partial^2 w_0}{\partial r^2} + \frac{1}{r}\frac{\partial w_0}{\partial r}\right)
\end{aligned} \tag{18-b}$$

Additionally, substituting Eq. (4-a) into the Eq. (13-b), the constitutive boundary condition can be obtained as follows:

$$\begin{aligned}
&\frac{\partial^2 u_0}{\partial r^2}(0,t) - \frac{1}{L}\frac{\partial u_0}{\partial r}(0,t) = 0 \quad , \quad \frac{\partial^2 u_0}{\partial r^2}(R,t) + \frac{1}{L}\frac{\partial u_0}{\partial r}(R,t) = 0,\\
&\frac{\partial^3 w_0}{\partial r^3}(0,t) - \frac{1}{L}\frac{\partial^2 w_0}{\partial r^2}(0,t) = 0 \quad , \quad \frac{\partial^3 w_0}{\partial r^3}(R,t) + \frac{1}{L}\frac{\partial^2 w_0}{\partial r^2}(R,t) = 0.
\end{aligned} \tag{19}$$

According to Eq. (18-a, b), it can be observed that by setting the parameter $L$ equal to zero, the equation of motion for a plate based on the local classical plate theory can be achieved.
Using Eqs. (5-b) and 16), the boundary condition can be obtained. The associated mathematical relations for different cases are given in Table 1.

**Table 1.** Boundary conditions and their mathematical relations.

| Location | B. Cs | Associated Mathematical relations |
|---|---|---|
| r=0 | Center of plate | $u_0 = w_0' = Q_r = 0$ |
| r=R | Clamped | $u_0 = w_0 = w_0' = 0$ |
| | Knife-edge support | $u_0 = w_0 = M_{rr} = 0$ |
| | Simply supported | $w_0 = N_r = M_r = 0$ |
| | Free | $Q_r = N_r = M_r = 0$ |

To obtain the appropriate solutions for $u_0(r, t)$ and $w_0(r, t)$, the oscillating responses were assumed to be:

$$\{u_0(r,t)\ ,\ w_0(r,t)\} = \{u(r)\ ,\ w(r)\}e^{i\omega_n t} \tag{20}$$

where $\omega_n$ is the natural frequency of the vibrating nano-plate. On using Eq. (20), Eqs. (18-a, b) and Eq. (19) can be recast into the following forms:

$$\begin{aligned}&\frac{A}{1-\nu^2}\left(\left\{\frac{d^2u}{dr^2}+\frac{1}{r}\frac{du}{dr}-\frac{1}{r^2}u\right\}-L^2\left\{\frac{d^4u}{dr^4}-\frac{\nu-1}{r}\frac{d^3u}{dr^3}\right\}\right)\\&\quad-\frac{B}{1-\nu^2}\left(\left\{\frac{d^3w}{dr^3}+\frac{1}{r}\frac{d^2w}{dr^2}-\frac{1}{r^2}\frac{dw}{dr}\right\}-L^2\left\{\frac{d^5w}{dr^5}-\frac{\nu-1}{r}\frac{d^4w}{dr^4}\right\}\right)=\left(I_1\frac{dw_0}{dr}-I_0u\right)\omega_n^2\end{aligned} \tag{21-a}$$

$$\begin{aligned}&\frac{B}{1-\nu^2}\left(\left\{\frac{d^3u}{dr^3}+\frac{2}{r}\frac{d^2u}{dr^2}-\frac{1}{r^2}\frac{du}{dr}+\frac{1}{r^3}u\right\}-L^2\left\{\frac{d^5u}{dr^5}-\frac{\nu-2}{r}\frac{d^4u}{dr^4}\right\}\right)\\&\quad-\frac{D}{1-\nu^2}\left(\left\{\frac{d^4w}{dr^4}+\frac{2}{r}\frac{d^3w}{dr^3}-\frac{1}{r^2}\frac{d^2w}{dr^2}+\frac{1}{r^3}\frac{dw}{dr}\right\}-L^2\left\{\frac{d^6w}{dr^6}-\frac{\nu-2}{r}\frac{d^5w}{dr^5}\right\}\right)\\&\qquad=\left(I_2\left(\frac{d^2w}{dr^2}+\frac{1}{r}\frac{dw}{dr}\right)-I_1\left(\frac{du}{dr}+\frac{1}{r}u\right)-I_0w\right)\omega_n^2\end{aligned} \tag{21-b}$$

$$\begin{aligned}&\frac{d^2u}{dr^2}(a)-\frac{1}{L}\frac{du}{dr}(a)=0\quad,\quad\frac{d^2u}{dr^2}(b)+\frac{1}{L}\frac{du}{dr}(b)=0.\\&\frac{d^3w}{dr^3}(a)-\frac{1}{L}\frac{d^2w}{dr^2}(a)=0\quad,\quad\frac{d^3w}{dr^3}(b)+\frac{1}{L}\frac{d^2w}{dr^2}(b)=0.\end{aligned} \tag{21-c}$$

To help to analyze the influence of effective parameters on the natural frequencies of the plate, the non-dimensional variables are defined as:

$$\begin{aligned}&(s,U,W,\bar{h},L_c)=\frac{1}{R}(r,u,w,h,L)\quad,\quad(\bar{A},\bar{B},\bar{D})=\left(\frac{AR^2}{D_0},\frac{BR}{D_0},\frac{D}{D_0}\right)\\&(\bar{I}_0,\bar{I}_1,\bar{I}_2)=\left(\frac{I_0}{I_{00}},\frac{I_1}{I_{00}R},\frac{I_2}{I_{00}R^2}\right)\quad,\quad\Omega_n^2=\frac{I_0R^4}{D}(1-\nu^2)\omega_n^2\end{aligned} \tag{22}$$

where $D_o$ and $I_{oo}$ are defined as:

$$D_0=\frac{E_mh^3}{12}\quad,\quad I_{00}=\rho_mh. \tag{23}$$

Substituting Eq. (22) into Eqs. (21-a, b, c), the non-dimensional governing equations and the corresponding constitutive boundary conditions are obtained as follows:

$$\begin{aligned}&\bar{A}\left(\left\{\frac{d^2U}{ds^2}+\frac{1}{s}\frac{dU}{ds}-\frac{1}{s^2}U\right\}-L_c^2\left\{\frac{d^4U}{ds^4}-\frac{\nu-1}{s}\frac{d^3U}{ds^3}\right\}\right)\\&\quad-\bar{\mathbf{B}}\left(\left\{\frac{d^3W}{ds^3}+\frac{1}{s}\frac{d^2W}{ds^2}-\frac{1}{s^2}\frac{dW}{ds}\right\}-L_c^2\left\{\frac{d^5W}{ds^5}-\frac{\nu-1}{s}\frac{d^4W}{ds^4}\right\}\right)=\left(\bar{I}_1\frac{dW}{ds}-\bar{I}_0U\right)\Omega_n^2\end{aligned} \tag{24-a}$$

$$\begin{aligned}&\bar{B}\left(\left\{\frac{d^3U}{ds^3}+\frac{2}{s}\frac{d^2U}{ds^2}-\frac{1}{s^2}\frac{dU}{ds}+\frac{1}{s^3}U\right\}-L_c^2\left\{\frac{d^5U}{dr^5}-\frac{\nu-2}{s}\frac{d^4U}{ds^4}\right\}\right)\\&\quad-\bar{D}\left(\left\{\frac{d^4W}{ds^4}+\frac{2}{s}\frac{d^3W}{ds^3}-\frac{1}{s^2}\frac{d^2W_0}{ds^2}+\frac{1}{s^3}\frac{dW_0}{ds}\right\}-L_c^2\left\{\frac{d^6W}{ds^6}-\frac{\nu-2}{s}\frac{d^5W}{ds^5}\right\}\right)\\&\qquad=\left(\bar{I}_2\left(\frac{d^2W}{ds^2}+\frac{1}{s}\frac{dW}{ds}\right)-\bar{I}_1\left(\frac{dU}{ds}+\frac{1}{s}U\right)-\bar{I}_0W\right)\Omega_n^2\end{aligned} \tag{24-b}$$

**Table 2.** Boundary conditions and their associated mathematical relations, based on the SDM.

| Location | B. Cs. | Associated Mathematical relations |
|---|---|---|
| s=0 | Center of plate | (1),(2) : $U=\frac{dW}{dr}=0$, (3) :$Q_r(0)=0\Rightarrow Q_r=0\Rightarrow \frac{\bar{B}}{1-\nu^2}\left(\frac{d^2U}{ds^2}-L_c^2\frac{d^4U}{ds^4}\right)-\frac{\bar{D}}{1-\nu^2}\left(\frac{d^3W}{ds^3}-L_c^2\frac{d^5W}{ds^5}\right)=0.$ |
| s=1 | Clamped | (1),(2),(3) : $U=W=\frac{dW}{dr}=0$ |
| | Knifed support | (1) ,(2) : $U=W=0$, (3): $M_{rr}=0\Rightarrow \frac{\bar{B}}{1-\nu^2}\left(\frac{dU}{ds}+\frac{\nu}{s}U-L_c^2\frac{d^3U}{ds^3}\right)-\frac{\bar{D}}{1-\nu^2}\left(\frac{d^2W}{ds^2}+\frac{\nu}{s}\frac{dW}{ds}-L_c^2\frac{d^4W}{ds^4}\right)=0.$ |
| | Simply supported | (1) : $W=0$, (2) ,(3) : $(N_{rr},M_{rr})=0\Rightarrow \frac{(\bar{A},\bar{B})}{1-\nu^2}\left(\frac{dU}{ds}+\frac{\nu}{s}U-L_c^2\frac{d^3U}{ds^3}\right)-\frac{(\bar{B},\bar{D})}{1-\nu^2}\left(\frac{d^2W}{ds^2}+\frac{\nu}{s}\frac{dW}{ds}-L_c^2\frac{d^4W}{ds^4}\right)=0,$ |
| | Free | (1) ,(2) : $(N_{rr},M_{rr})=0\Rightarrow \frac{(\bar{A},\bar{B})}{1-\nu^2}\left(\frac{dU}{ds}+\frac{\nu}{s}U-L^2\frac{d^3U}{ds^3}\right)-\frac{(\bar{B},\bar{D})}{1-\nu^2}\left(\frac{d^2W}{ds^2}+\frac{\nu}{s}\frac{dW}{ds}-L^2\frac{d^4W}{ds^4}\right)=0,$ (3) : $Q_r=0\Rightarrow \frac{\bar{B}}{1-\nu^2}\left(\frac{d^2U}{ds^2}+\frac{1}{s}\frac{dU}{ds}-\frac{1}{s^2}U-L^2\left(\frac{d^4U}{ds^4}-\frac{\nu-1}{s}\frac{d^3U}{ds^3}\right)\right)-\frac{\bar{D}}{1-\nu^2}\left(\frac{d^3W}{ds^3}+\frac{1}{s}\frac{d^2W}{ds^2}-\frac{1}{s^2}\frac{dW}{ds}-L^2\left(\frac{d^5W}{ds^5}-\frac{\nu-1}{s}\frac{d^4W}{ds^4}\right)\right)=0.$ |

$$\frac{d^2U}{ds^2}(0)-\frac{1}{L_c}\frac{dU}{ds}(0)=0 \quad , \quad \frac{d^2U}{ds^2}(1)+\frac{1}{L_c}\frac{dU}{ds}(1)=0,$$
$$\frac{d^3W}{ds^3}(0)-\frac{1}{L_c}\frac{d^2W}{ds^2}(0)=0 \quad , \quad \frac{d^3W}{ds^3}(1)+\frac{1}{L_c}\frac{d^2W}{ds^2}(1)=0. \tag{24-c}$$

Also, on using Eq. (16) and Eq. (22), the boundary conditions given in Table 1 can be recast in a non-dimensional form as in Table 2, based on the clamped, knife-edge, simply supported and free edges, respectively.

### 2.2. Equations of motion based on the strain-gradient theory (SGT)

To check and verify the versatility of the SDM for modeling and analyzing the vibrational behavior of the annular nano-plate, in this section, the governing equations of motion based on the SGT are derived. Using the strain-gradient theory, SGT, and Kirchhoff's plate model, the stress components are given by [62];

$$\sigma_{rr}=\sigma_{rr}^{(0)}-\left\{\frac{\partial}{\partial r}\sigma_{rrr}^{(1)}+\frac{1}{r}\left(\sigma_{rrr}^{(1)}-\sigma_{\theta\theta r}^{(1)}+\sigma_{r\theta\theta}^{(1)}\right)\right\},$$
$$\sigma_{\theta\theta}=\sigma_{\theta\theta}^{(0)}-\left\{\frac{\partial}{\partial r}\sigma_{r\theta\theta}^{(1)}+\frac{1}{r}\left(2\sigma_{r\theta\theta}^{(1)}+\sigma_{\theta\theta r}^{(1)}\right)\right\}. \tag{26}$$

In Eq. (26), the superscript (0) and (1) denote the zero and first order of stress tensor in the SGT. Also, the non-zero component of these tensors are as follows:

$$\begin{cases}\sigma_{rr}^{(0)}=E\left(\varepsilon_{rr}+\nu\varepsilon_{\theta\theta}\right)\\ \sigma_{\theta\theta}^{(0)}=E\left(\nu\varepsilon_{rr}+\varepsilon_{\theta\theta}\right)\end{cases} , \quad \begin{cases}\sigma_{rrr}^{(1)}=EL^2\left(\varepsilon_{rrr}+\nu\varepsilon_{\theta\theta r}\right)\\ \sigma_{\theta\theta r}^{(1)}=EL^2\left(\nu\varepsilon_{rrr}+\varepsilon_{\theta\theta r}\right).\\ \sigma_{r\theta\theta}^{(1)}=EL^2\left(1-\nu^2\right)\varepsilon_{r\theta\theta}\end{cases} \tag{27}$$

where, $L$ is the material length-scale, and the strain components as well as the strain gradient tensors are defined as follows:

$$\begin{cases}\varepsilon_{rr}=\frac{\partial u_r}{\partial r}=\frac{\partial u_0}{\partial r}-z\frac{\partial^2 w_0}{\partial r^2}\\ \varepsilon_{\theta\theta}=\frac{u_r}{r}=\frac{1}{r}u_0(r,t)-z\frac{1}{r}\frac{\partial w_0}{\partial r}\end{cases} , \quad \begin{cases}\varepsilon_{rrr}=\frac{\partial\varepsilon_{rr}}{\partial r}=\frac{\partial^2 u_0}{\partial r^2}-z\frac{\partial^3 w_0}{\partial r^3}\\ \varepsilon_{\theta\theta r}=\frac{\partial\varepsilon_{\theta\theta}}{\partial r}=\frac{1}{r}\frac{\partial u_0}{\partial r}-\frac{1}{r^2}u_0-z\frac{1}{r}\frac{\partial^2 w_0}{\partial r^2}+z\frac{1}{r^2}\frac{\partial w_0}{\partial r}\\ \varepsilon_{r\theta\theta}=\frac{1}{r}\left(\frac{\partial}{\partial r}(r\varepsilon_{\theta\theta})-\varepsilon_{\theta\theta}\right)=\frac{1}{r}\frac{\partial u_0}{\partial r}-\frac{1}{r^2}u_0-z\frac{1}{r}\frac{\partial^2 w_0}{\partial r^2}+z\frac{1}{r^2}\frac{\partial w_0}{\partial r}\end{cases} . \tag{28}$$

Using Eq. (4), Eqs. (26-28), the stress and moment resultant can be written as:

$$\{N_{rr},M_{rr}\}=\{A,B\}\left\{\left(\frac{\partial u_0}{\partial r}+\frac{\nu}{r}u_0\right)-L^2\left(\frac{\partial^3 u_0}{\partial r^3}+\frac{1}{r}\frac{\partial^2 u_0}{\partial r^2}-\frac{2}{r^2}\frac{\partial u_0}{\partial r}+\frac{2}{r^3}u_0\right)\right\}$$
$$-\{B,D\}\left\{\left(\frac{\partial^2 w_0}{\partial r^2}+\frac{\nu}{r}\frac{\partial w_0}{\partial r}\right)-L^2\left(\frac{\partial^4 w_0}{\partial r^4}+\frac{1}{r}\frac{\partial^3 w_0}{\partial r^3}-\frac{2}{r^2}\frac{\partial^2 w_0}{\partial r^2}+\frac{2}{r^3}\frac{\partial w_0}{\partial r}\right)\right\}, \tag{29}$$

$$\{N_{\theta\theta},M_{\theta\theta}\}==\{A,B\}\left\{\left(\nu\frac{\partial u_0}{\partial r}+\frac{1}{r}u_0\right)-L^2\left(\frac{1}{r}\frac{\partial^2 u_0}{\partial r^2}+\frac{1}{r^2}\frac{\partial u_0}{\partial r}-\frac{1}{r^3}u_0\right)\right\}$$
$$-\{B,D\}\left\{\left(\nu\frac{\partial^2 w_0}{\partial r^2}+\frac{1}{r}\frac{\partial w_0}{\partial r}\right)-L^2\left(\frac{1}{r}\frac{\partial^3 w_0}{\partial r^3}+\frac{1}{r^2}\frac{\partial^2 w_0}{\partial r^2}-\frac{1}{r^3}\frac{\partial w_0}{\partial r}\right)\right\},$$

(29-cont.)

$$Q_r=B\left\{\left(\frac{\partial^2 u_0}{\partial r^2}+\frac{1}{r}\frac{\partial u_0}{\partial r}-\frac{1}{r^2}u_0\right)-L_c^2\left(\frac{\partial^4 u_0}{\partial r^4}+\frac{2}{r}\frac{\partial^3 u_0}{\partial r^3}-\frac{3}{r^2}\frac{\partial^2 u_0}{\partial r^2}+\frac{3}{r^3}\frac{\partial u_0}{\partial r}-\frac{3}{r^4}u_0\right)\right\}$$
$$-\bar{D}\left\{\left(\frac{\partial^3 w_0}{\partial r^3}+\frac{1}{r}\frac{\partial^2 w_0}{\partial r^2}-\frac{1}{r^2}\frac{\partial w_0}{\partial r}\right)-L_c^2\left(\frac{\partial^5 w_0}{\partial r^5}+\frac{2}{r}\frac{\partial^4 w_0}{\partial r^4}-\frac{3}{r^2}\frac{\partial^3 w_0}{\partial r^3}+\frac{3}{r^3}\frac{\partial^2 w_0}{\partial r^2}-\frac{3}{r^4}\frac{\partial w_0}{\partial r}\right)\right\}=0.$$

Substituting Eqs. (29) into the Eq. (5-a) and using Eqs. (20) and (22-23), the equations of motion for the circular FGM nano-plate based on the SGT are derived as:

$$\bar{A}\left(\frac{d^2U}{ds^2}+\frac{1}{s}\frac{\partial U}{\partial r}-\frac{1}{r^2}U\right)+\bar{B}\left(\frac{d^3w_0}{ds^3}+\frac{1}{s}\frac{d^2w_0}{ds^2}-\frac{1}{s^2}\frac{dw_0}{ds}\right)$$
$$-\bar{A}L_c^2\left(\frac{d^4U}{ds^4}+\frac{2}{s}\frac{d^3U}{ds^3}-\frac{3}{s^2}\frac{d^2U}{ds^2}+\frac{3}{s^3}\frac{dU}{ds}-\frac{3}{s^4}U\right)$$
$$-\bar{B}L_c^2\left(\frac{d^5W}{ds^5}+\frac{2}{s}\frac{d^4W}{ds^4}-\frac{3}{s^2}\frac{d^3W}{ds^3}+\frac{3}{s^3}\frac{d^2W}{ds^2}-\frac{3}{s^4}\frac{dW}{ds}\right)=\left(\bar{I}_1\frac{dW}{ds}-\bar{I}_0U\right)\Omega_n^2 \tag{30-a}$$

$$\bar{B}\left(\frac{d^3U}{ds^3}+\frac{2}{s}\frac{d^2U}{ds^2}-\frac{1}{s^2}\frac{dU}{ds}+\frac{1}{s^3}U\right)+\bar{D}\left(\frac{d^4W}{ds^4}+\frac{2}{s}\frac{d^3W}{\partial s^3}-\frac{1}{s^2}\frac{d^2W}{\partial s^2}+\frac{1}{s^3}\frac{dW}{\partial s}\right)$$
$$-\bar{B}L_c^2\left(\frac{d^5U}{ds^5}+\frac{3}{s}\frac{d^4U}{ds^4}-\frac{3}{s^2}\frac{d^3U}{ds^3}+\frac{6}{s^3}\frac{d^2U}{ds^2}-\frac{9}{s^4}\frac{dU}{ds}+\frac{9}{s^5}U\right)$$
$$-\bar{D}L_c^2\left(\frac{d^6W}{ds^6}+\frac{3}{s}\frac{d^5W}{ds^5}-\frac{3}{s^2}\frac{d^4W}{ds^4}+\frac{6}{s^3}\frac{d^3W}{ds^3}-\frac{9}{s^4}\frac{d^2W}{ds^2}+\frac{9}{s^5}\frac{dW}{ds}\right)$$
$$=\left(\bar{I}_2\left(\frac{d^2W}{ds^2}+\frac{1}{s}\frac{dW}{ds}\right)-\bar{I}_1\left(\frac{dU}{ds}+\frac{1}{s}U\right)-\bar{I}_0W\right)\Omega_n^2 \tag{30-b}$$

**Table 3.** Mathematical relations in the frequency domain for the B. Cs of the nanoplate based on the SGT.

| Location | B. Cs. | Associated Mathematical relations |
|---|---|---|
| s=0 | Center of plate | $(1),(2):\ U=\frac{dW}{dr}=0,\quad (3):Q_r(0)=0\Rightarrow \bar{B}\left(\frac{d^2U}{ds^2}-L_c^2\frac{d^4U}{ds^4}\right)-\bar{D}\left(\frac{d^3W}{ds^3}-L_c^2\frac{d^5W}{ds^5}\right)=0.$ |
| s=1 | Clamped | $(1),(2),(3):\ U=W=\frac{dW}{dr}=0$ |
| s=1 | Knife-edge support | $(1),(2):\ U=W=0\ ,\ (3):M_{rr}=0\Rightarrow \bar{B}\left\{\left(\frac{dU}{ds}+\frac{\nu}{s}U\right)-L_c^2\left\{\frac{d^3U}{dr^3}+\frac{1}{s}\frac{d^2U}{ds^2}-\frac{2}{s^2}\frac{dU}{ds}+\frac{2}{s^3}U\right\}\right\}$ $-\bar{D}\left\{\left(\frac{d^2W}{ds^2}+\frac{\nu}{s}\frac{dW}{ds}\right)-L_c^2\left(\frac{d^4W}{ds^4}+\frac{1}{s}\frac{d^3W}{ds^3}-\frac{2}{s^2}\frac{d^2W}{ds^2}+\frac{2}{s^3}\frac{dW}{ds}\right)\right\}=0.$ |
| s=1 | Simply supported | $(1):W=0,\quad (2),(3):(N_{rr},M_{rr})=0\Rightarrow(\bar{A},\bar{B})\left\{\left(\frac{dU}{ds}+\frac{\nu}{s}u_0\right)-L_c^2\left\{\frac{d^3U}{ds^3}+\frac{1}{s}\frac{d^2U}{ds^2}-\frac{2}{s^2}\frac{dU}{ds}+\frac{2}{s^3}U\right\}\right\}$ $-(\bar{B},\bar{D})\left\{\left(\frac{d^2W}{ds^2}+\frac{\nu}{s}\frac{dW}{ds}\right)-L_c^2\left(\frac{d^4W}{ds^4}+\frac{1}{s}\frac{d^3W}{ds^3}-\frac{2}{s^2}\frac{d^2W}{ds^2}+\frac{2}{s^3}\frac{dW}{ds}\right)\right\}=0.$ |
| s=1 | Free | $(1),(2):(N_{rr},M_{rr})=0\Rightarrow(\bar{A},\bar{B})\left\{\left(\frac{dU}{ds}+\frac{\nu}{s}u_0\right)-L_c^2\left\{\frac{d^3U}{ds^3}+\frac{1}{s}\frac{d^2U}{ds^2}-\frac{2}{s^2}\frac{dU}{ds}+\frac{2}{s^3}U\right\}\right\}$ $-(\bar{B},\bar{D})\left\{\left(\frac{d^2W}{ds^2}+\frac{\nu}{s}\frac{dW}{ds}\right)-L_c^2\left(\frac{d^4W}{ds^4}+\frac{1}{s}\frac{d^3W}{ds^3}-\frac{2}{s^2}\frac{d^2W}{ds^2}+\frac{2}{s^3}\frac{dW}{ds}\right)\right\}=0,$ $(3):Q_r=0\Rightarrow\bar{B}\left\{\left(\frac{d^2U}{ds^2}+\frac{1}{s}\frac{dU}{dr}-\frac{1}{s^2}U\right)-L_c^2\left(\frac{d^4U}{ds^4}+\frac{2}{s}\frac{d^3U}{ds^3}-\frac{3}{s^2}\frac{d^2U}{ds^2}+\frac{3}{s^3}\frac{dU}{ds}-\frac{3}{s^4}U\right)\right\}$ $-\bar{D}\left[\left(\frac{d^3W}{ds^3}+\frac{1}{s}\frac{d^2W}{ds^2}-\frac{1}{s^2}\frac{dW}{ds}\right)-L_c^2\left(\frac{d^5W}{ds^5}+\frac{2}{s}\frac{d^4W}{ds^4}-\frac{3}{s^2}\frac{d^3W}{ds^3}+\frac{3}{s^3}\frac{d^2W}{ds^2}-\frac{3}{s^4}\frac{dW}{ds}\right)\right]=0.$ |

Also, using the concepts on Ref. [61], and Eqs. (20) and (22), the higher-order boundary conditions are:

$$@s=0:\begin{cases}\bar{A}\dfrac{d^2U}{ds^2}-\bar{B}\dfrac{d^3W}{ds^3}=0,\\ \bar{B}\dfrac{d^2U}{ds^2}-\bar{D}\dfrac{d^3W}{ds^3}=0,\end{cases}\quad,\quad @s=1:\begin{cases}\bar{A}\left(\dfrac{d^2U}{ds^2}+\nu\left(\dfrac{dU}{ds}-U\right)\right)-\bar{B}\left(\dfrac{d^3W}{ds^3}+\nu\left(\dfrac{d^2W}{ds^2}-\dfrac{dW}{ds}\right)\right)=0\\ \bar{B}\left(\dfrac{d^2U}{ds^2}+\nu\left(\dfrac{dU}{ds}-U\right)\right)-\bar{D}\left(\dfrac{d^3W}{ds^3}+\nu\left(\dfrac{d^2W}{ds^2}-\dfrac{dW}{ds}\right)\right)=0\end{cases} \tag{30-c}$$

On using Eq. (22), the boundary conditions given in Table 1 can be recast in a non-dimensional form in the frequency domain as in Table 3, based on the clamped, knife-edge, simply supported, and free edges, respectively.

## 3. Solution Procedure using the Generalized Differential Quadrature Rule (GDQR)

The GDQR has been used as a general numerical method to solve the high-order differential equations related to the Euler beam and plate fourth-order differential equations [63]. In the present work, the free vibration of the circular FGM nano-plate is governed by a set of sixth-order differential equations, that is constrained by five boundary conditions on each edge.

According to this method, the $n^{th}$ order derivatives of functions $U(s)$ and $W(s)$ at any discrete point in a domain are approximated by the weighted linear sum of the function values at all other discrete points $s = s_i$ ($i$ =1, 2,…, $N$) [63] such that:

$$\begin{aligned}U^{(n)}(s_i)&=\sum_{k=0}^{1}g_{1k}^{(n)}(s_i)U_1^{(k)}+\sum_{j=2}^{N-1}g_{j0}^{(n)}(s_i)U_j^{(k)}+\sum_{k=0}^{1}g_{Nk}^{(n)}(s_i)U_N^{(k)}=\sum_{k=1}^{N+2}E_{ik}^{(n)}\Psi_k\\ W^{(n)}(s_i)&=\sum_{k=0}^{2}h_{1k}^{(n)}(s_i)W_1^{(k)}+\sum_{j=2}^{N-1}h_{j0}^{(n)}(s_i)W_j^{(k)}+\sum_{k=0}^{2}h_{Nk}^{(n)}(s_i)W_N^{(k)}=\sum_{k=1}^{N+4}F_{ik}^{(n)}\Theta_k\end{aligned} \tag{31}$$

where

$$\begin{aligned}\left\{E_{ik}^{(n)}\right\}^T&=\left\{g_{10}^{(n)}(r_i),g_{11}^{(n)}(r_i),g_{20}^{(n)}(r_i),\ldots,g_{(N-1)0}^{(n)}(r_i),g_{N0}^{(n)}(r_i),g_{N1}^{(n)}(r_i)\right\}\\ \left\{F_{ik}^{(n)}\right\}^T&=\left\{h_{10}^{(n)}(r_i),h_{11}^{(n)}(r_i),h_{12}^{(n)}(r_i),h_{20}^{(n)}(r_i),\ldots,h_{(N-1)0}^{(n)}(r_i),h_{N0}^{(n)}(r_i),h_{N1}^{(n)}(r_i),h_{N2}^{(n)}(r_i)\right\}\end{aligned} \tag{32-a}$$

$$\begin{aligned}\left\{\Psi_1,\Psi_2,\ldots,\Psi_j,\ldots,\Psi_{N+2}\right\}&=\left\{U_1,U_1^{(1)},U_2,\ldots,U_N,U_N^{(1)}\right\}\\ \left\{\Theta_1,\Theta_2,\ldots,\Theta_j,\ldots,\Theta_{N+4}\right\}&=\left\{W_1,W_1^{(1)},W_1^{(2)},W_2,\ldots,W_N,W_N^{(1)},W_N^{(2)}\right\}\end{aligned} \tag{32-b}$$

$$s_i=\frac{1}{2}\left(1-\cos\left(\frac{i-1}{N-1}\pi\right)\right) \tag{32-c}$$

Moreover, the weighting coefficients in Eqs. (32-a) and (32-b) are defined as follows:

$$\begin{cases}g_{ki}(x)=\left(a_{ki}x^2+b_{ki}x+c_{ki}\right)L_1(x) & (i=0,1),(k=1,N)\\ g_{j0}(x)=\dfrac{(x-x_1)(x-x_N)}{(x_j-x_1)(x_j-x_N)}L_j(x) & (j=2,3,\ldots,N-1)\end{cases} \tag{33-a}$$

$$\begin{cases}h_{ki}(x)=\dfrac{(x-x_N)^2}{(x_1-x_N)^2}\left(\bar{a}_{ki}x^2+\bar{b}_{ki}x+\bar{c}_{ki}\right)L_1(x) & (i=0,1,2),(k=1,N)\\ h_{j0}(x)=\dfrac{(x-x_1)^2(x-x_N)^2}{(x_j-x_1)^2(x_j-x_N)^2}L_j(x) & (j=2,3,\ldots,N-1)\end{cases} \tag{33-b}$$

where

$$\begin{cases}a_{10}=\dfrac{-1}{(x_1-x_N)^2}-\dfrac{L_1^{(1)}(x_1)}{(x_1-x_N)}\ ,\ b_{10}=\dfrac{1}{(x_1-x_N)}-a_{10}(x_1+x_N)\ ,\ c_{10}=1-a_{10}x_1^2-b_{10}x_1\ ,\\ a_{11}=\dfrac{1}{(x_1-x_N)}\ ,\ b_{10}=-\dfrac{(x_1+x_N)}{(x_1-x_N)}\ ,\ c_{10}=\dfrac{x_1x_N}{(x_1-x_N)},\end{cases} \tag{34-a}$$

$$\begin{cases}a_{N0}=\dfrac{-1}{(x_1-x_N)^2}+\dfrac{L_1^{(N)}(x_N)}{(x_1-x_N)}\ ,\ b_{N0}=\dfrac{-1}{(x_1-x_N)}-a_{N0}(x_1+x_N)\ ,\ c_{N0}=1-a_{N0}x_N^2-b_{N0}x_N\ ,\\ a_{N1}=\dfrac{-1}{(x_1-x_N)}\ ,\ b_{N0}=\dfrac{(x_1+x_N)}{(x_1-x_N)}\ ,\ c_{N0}=\dfrac{-x_1x_N}{(x_1-x_N)}.\end{cases} \tag{34-b}$$

$$
\begin{cases}
\bar{a}_{10}=\left(L_1^{(1)}(x_1)+\dfrac{2}{x_1-x_N}\right)^2-\dfrac{L_1^{(2)}(x_1)}{2}-\dfrac{1}{(x_1-x_N)^2}-\dfrac{2L_1^{(1)}(x_1)}{x_1-x_N} \\
\bar{b}_{10}=-\left(L_1^{(1)}(x_1)+\dfrac{2}{x_1-x_N}\right)-2\bar{a}_{10}x_1\ ,\quad c_{10}=1+\bar{a}_{10}x_1^2+x_1\left(L_1^{(1)}(x_1)+\dfrac{2}{x_1-x_N}\right) \\
\bar{a}_{11}=-\left(L_1^{(1)}(x_1)+\dfrac{2}{x_1-x_N}\right)^2,\ \bar{b}_{11}=1-2\bar{a}_{10}x_1,\ \bar{c}_{11}=x_1(\bar{a}_{11}x_1-1),\ \bar{a}_{12}=\dfrac{1}{2},\ \bar{b}_{12}=-x_1,\ \bar{c}_{12}=\dfrac{x_1^2}{2}, \\
\bar{a}_{N0}=\left(L_N^{(1)}(x_N)-\dfrac{2}{x_1-x_N}\right)^2-\dfrac{L_N^{(2)}(x_N)}{2}-\dfrac{1}{(x_1-x_N)^2}+\dfrac{2L_N^{(1)}(x_N)}{x_1-x_N}, \\
\bar{b}_{N0}=-\left(L_N^{(1)}(x_N)-\dfrac{2}{x_1-x_N}\right)-2\bar{a}_{N0}x_N\ ,\ c_{N0}=1+\bar{a}_{N0}x_N^2+x_N\left(L_N^{(1)}(x_N)-\dfrac{2}{x_1-x_N}\right), \\
\bar{a}_{N1}=-\left(L_N^{(1)}(x_N)-\dfrac{2}{x_1-x_N}\right)^2,\ \bar{b}_{N1}=1-2\bar{a}_{N0}x_N,\ \bar{c}_{N1}=x_N(\bar{a}_{N1}x_N-1), \\
\bar{a}_{N2}=\dfrac{1}{2},\ \bar{b}_{N2}=-x_N,\ \bar{c}_{N2}=\dfrac{x_N^2}{2}.
\end{cases}
\tag{34-c}
$$

In Eq. (34-c), $L(x)$ is a Lagrange interpolation function with the following properties [63];

$$
L_i(x_j)=\begin{cases}1 & i=j\\ 0 & i\neq j\end{cases}
\tag{35}
$$

Note that the first and second derivatives of the Lagrange interpolation function have been explicitly obtained in [64, 65].

### 3.1. Discretization of the motion equations based on the SDM using the GDQR method

Using Eq. (31), the equation of motion and the constitutive boundary conditions, Eq. (24-a, b, c) can be written into the following forms:

$$
\begin{aligned}
&\bar{A}\left(\left\{\sum_{k=1}^{N+4}E_{ik}^{(2)}\Psi_k+\frac{1}{s_i}\sum_{k=1}^{N+4}E_{ik}^{(1)}\Psi_k-\frac{1}{s_i^2}U_i\right\}-L_c^2\left\{\sum_{k=1}^{N+4}E_{ik}^{(4)}\Psi_k-\frac{\nu-1}{s_i}\sum_{k=1}^{N+4}E_{ik}^{(3)}\Psi_k\right\}\right)\\
&-\bar{B}\left(\left\{\sum_{k=1}^{N+4}F_{ik}^{(3)}\Theta_k+\frac{1}{s_i}\sum_{k=1}^{N+4}F_{ik}^{(2)}\Theta_k-\frac{1}{s_i^2}\sum_{k=1}^{N+4}F_{ik}^{(1)}\Theta_k\right\}-L_c^2\left\{\sum_{k=1}^{N+4}F_{ik}^{(5)}\Theta_k-\frac{\nu-1}{s_i}\sum_{k=1}^{N+4}F_{ik}^{(4)}\Theta_k\right\}\right)\\
&\qquad=\left(\bar{I}_1\sum_{k=1}^{N+4}F_{ik}^{(1)}\Theta_k-\bar{I}_0U_i\right)\Omega_n^2
\end{aligned}
\tag{36-a}
$$

$$
\begin{aligned}
&\bar{B}\left(\left\{\sum_{k=1}^{N+4}E_{ik}^{(3)}\Psi_k+\frac{2}{s_i}\sum_{k=1}^{N+4}E_{ik}^{(2)}\Psi_k-\frac{1}{s_i^2}\sum_{k=1}^{N+4}E_{ik}^{(1)}\Psi_k+\frac{1}{s_i^3}U\right\}-L_c^2\left\{\sum_{k=1}^{N+4}E_{ik}^{(5)}\Psi_k-\frac{\nu-2}{s_i}\sum_{k=1}^{N+4}E_{ik}^{(4)}\Psi_k\right\}\right)\\
&-\bar{D}\left(\left\{\sum_{k=1}^{N+4}F_{ik}^{(4)}\Theta_k+\frac{2}{s_i}\sum_{k=1}^{N+4}F_{ik}^{(3)}\Theta_k-\frac{1}{s_i^2}\sum_{k=1}^{N+4}F_{ik}^{(2)}\Theta_k+\frac{1}{s_i^3}\sum_{k=1}^{N+4}F_{ik}^{(1)}\Theta_k\right\}-L_c^2\left\{\sum_{k=1}^{N+4}F_{ik}^{(6)}\Theta_k-\frac{\nu-2}{s_i}\sum_{k=1}^{N+4}F_{ik}^{(5)}\Theta_k\right\}\right)\\
&\qquad=\left(\bar{I}_2\left(\sum_{k=1}^{N+4}F_{ik}^{(2)}\Theta_k+\frac{1}{s_i}\sum_{k=1}^{N+4}F_{ik}^{(1)}\Theta_k\right)-\bar{I}_1\left(\sum_{k=1}^{N+4}E_{ik}^{(1)}\Psi_k+\frac{1}{s_i}U\right)-\bar{I}_0W_i\right)\Omega_n^2
\end{aligned}
\tag{36-b}
$$

$$
\begin{aligned}
&\sum_{k=1}^{N+4}E_{1k}^{(2)}\Psi_k-\frac{1}{L_c}\sum_{k=1}^{N+4}E_{1k}^{(1)}\Psi_k=0\quad,\quad\sum_{k=1}^{N+4}E_{Nk}^{(2)}\Psi_k+\frac{1}{L_c}\sum_{k=1}^{N+4}E_{Nk}^{(1)}\Psi_k=0\ ,\\
&\sum_{k=1}^{N+4}F_{1k}^{(3)}\Theta_k-\frac{1}{L_c}\sum_{k=1}^{N+4}F_{1k}^{(2)}\Theta_k=0\quad,\quad\sum_{k=1}^{N+4}F_{Nk}^{(3)}\Theta_k+\frac{1}{L_c}\sum_{k=1}^{N+4}F_{Nk}^{(2)}\Theta_k=0\ .
\end{aligned}
\tag{36-c}
$$

Using Eq. (31) and Table 2, the corresponding associated mathematical relations for the boundary conditions are obtained and listed in Table 4, based on the SDM.

### 3.2. Discretization of the motion equations based on the SGT using the GDQR method

Using Eq. (31), the equations of motion, Eq. (30-a,b) and higher boundary conditions, Eq. (31-a, b), can be written as:

$$
\bar{A}L_c^2\left(\sum_{k=1}^{N+4}E_{1k}^{(2)}\Psi_k+\nu\left(\frac{1}{s_i}\sum_{k=1}^{N+4}E_{1k}^{(1)}\Psi_k-\frac{1}{s_i^2}U_i\right)\right)-\bar{B}L_c^2\left(\sum_{k=1}^{N+4}F_{1k}^{(3)}\Theta_k+\nu\left(\frac{1}{s_i}\sum_{k=1}^{N+4}F_{1k}^{(2)}\Theta_k-\frac{1}{s_i^2}\sum_{k=1}^{N+4}F_{1k}^{(2)}\Theta_k\right)\right)=0,
\tag{37}
$$

$$
\bar{B}L_c^2\left(\sum_{k=1}^{N+4}E_{1k}^{(2)}\Psi_k+\nu\left(\frac{1}{s_i}\sum_{k=1}^{N+4}E_{1k}^{(1)}\Psi_k-\frac{1}{s_i^2}U_i\right)\right)-\bar{D}L_c^2\left(\sum_{k=1}^{N+4}F_{1k}^{(3)}\Theta_k+\nu\left(\frac{1}{s_i}\sum_{k=1}^{N+4}F_{1k}^{(2)}\Theta_k-\frac{1}{s_i^2}\sum_{k=1}^{N+4}F_{1k}^{(2)}\Theta_k\right)\right)=0.
\tag{38}
$$

Also, using Eq. (31) and Table 3, the corresponding associated mathematical relations for the boundary conditions based on the SDM are obtained and listed in Table 4.

**Table 4.** Mathematical relations for the B. Cs of the nanoplate, based on SDM.

| Location | B. Cs. | Associated Mathematical relations |
|---|---|---|
| s=0 | Center of plate | $(1): U_1 = 0 \;,\; (2): \sum_{k=1}^{N+4} F_{1k}^{(1)}\Theta_k = 0 \;,$ $(3): \overline{B}\left(\sum_{k=1}^{N+4} E_{1k}^{(2)}\Psi_k - L_c^2\sum_{k=1}^{N+4} E_{1k}^{(4)}\Psi_k\right) - \overline{D}\left(\sum_{k=1}^{N+4} F_{1k}^{(3)}\Theta_k - L_c^2\sum_{k=1}^{N+4} F_{1k}^{(5)}\Theta_k\right) = 0.$ |
| s=1 | Clamped | $(1): U_N = 0 \;,\; (2): W_N = 0 \;,\; (3): \sum_{k=1}^{N+4} F_{Nk}^{(1)}\Theta_k = 0.$ |
| | Knife-edge support | $(1): U_N = 0 \;,\; (2): W_N = 0 \,,$ $(3): M_{rr} = 0 \Rightarrow \overline{B}\left(\sum_{k=1}^{N+4} E_{Nk}^{(1)}\Psi_k + \nu U_N - L_c^2\sum_{k=1}^{N+4} E_{Nk}^{(3)}\Psi_k\right) - \overline{D}\left(\sum_{k=1}^{N+4} F_{Nk}^{(2)}\Theta_k + \nu\sum_{k=1}^{N+4} F_{Nk}^{(1)}\Theta_k - L_c^2\sum_{k=1}^{N+4} F_{Nk}^{(4)}\Theta_k\right) = 0.$ |
| | Simply supported | $(1): W_N = 0,$ $(2)\,,\,(3): (N_{rr}, M_{rr}) = 0 \Rightarrow (\overline{A}, \overline{B})\left(\sum_{k=1}^{N+4} E_{Nk}^{(1)}\Psi_k + \nu U_N - L_c^2\sum_{k=1}^{N+4} E_{Nk}^{(3)}\Psi_k\right) - (\overline{B}, \overline{D})\left(\sum_{k=1}^{N+4} F_{Nk}^{(2)}\Theta_k + \nu\sum_{k=1}^{N+4} F_{Nk}^{(1)}\Theta_k - L_c^2\sum_{k=1}^{N+4} F_{Nk}^{(4)}\Theta_k\right) = 0.$ |
| | Free | $(1): Q_r = 0 \Rightarrow \overline{B}\left(\sum_{k=1}^{N+4} E_{Nk}^{(1)}\Psi_k + \nu U_N - L_c^2\sum_{k=1}^{N+4} E_{Nk}^{(3)}\Psi_k\right) - \overline{D}\left(\sum_{k=1}^{N+4} F_{Nk}^{(2)}\Theta_k + \nu\sum_{k=1}^{N+4} F_{Nk}^{(1)}\Theta_k - L_c^2\sum_{k=1}^{N+4} F_{Nk}^{(4)}\Theta_k\right) = 0,$ $(2)\,,\,(3): (N_{rr}, M_{rr}) = 0 \Rightarrow (\overline{A}, \overline{B})\left(\sum_{k=1}^{N+4} E_{Nk}^{(1)}\Psi_k + \nu U_N - L_c^2\sum_{k=1}^{N+4} E_{Nk}^{(3)}\Psi_k\right) - (\overline{B}, \overline{D})\left(\sum_{k=1}^{N+4} F_{Nk}^{(2)}\Theta_k + \nu\sum_{k=1}^{N+4} F_{Nk}^{(1)}\Theta_k - L_c^2\sum_{k=1}^{N+4} F_{Nk}^{(4)}\Theta_k\right) = 0.$ |

**Table 5.** Mathematical relations for the B. Cs of the nanoplate, based on SGT.

| Location | B. Cs. | Associated Mathematical relations |
|---|---|---|
| s=0 | Center of plate | $(1): U_1 = 0 \;,\; (2): \sum_{k=1}^{N+4} F_{1k}^{(1)}\Theta_k = 0 \;,$ $(3): Q_r = 0 \Rightarrow \overline{B}\left(\sum_{k=1}^{N+4} E_{1k}^{(2)}\Psi_k - L_c^2\sum_{k=1}^{N+4} E_{1k}^{(4)}\Psi_k\right) - \overline{D}\left(\sum_{k=1}^{N+4} F_{1k}^{(3)}\Theta_k - L_c^2\sum_{k=1}^{N+4} F_{1k}^{(5)}\Theta_k\right) = 0.$ |
| s=1 | Clamped | $(1): U_N = 0 \;,\; (2): W_N = 0 \;,\; (3): \sum_{k=1}^{N+4} F_{Nk}^{(1)}\Theta_k = 0.$ |
| | Knife-edge support | $(1): U_N = 0 \;,\; (2): W_N = 0 \,,$ $(3): M_{rr} = 0 \Rightarrow \overline{B}\left(\sum_{k=1}^{N+4} E_{Nk}^{(1)}\Psi_k + \nu U_N - L_c^2\left\{\sum_{k=1}^{N+4} E_{Nk}^{(3)}\Psi_k + \sum_{k=1}^{N+4} E_{Nk}^{(2)}\Psi_k - 2\sum_{k=1}^{N+4} E_{Nk}^{(2)}\Psi_k + 2U_i\right\}\right)$ $- \overline{D}\left(\sum_{k=1}^{N+4} F_{Nk}^{(2)}\Theta_k + \nu\sum_{k=1}^{N+4} F_{Nk}^{(1)}\Theta_k - L_c^2\left\{\sum_{k=1}^{N+4} F_{Nk}^{(4)}\Theta_k + \sum_{k=1}^{N+4} F_{Nk}^{(3)}\Theta_k - 2\sum_{k=1}^{N+4} F_{Nk}^{(2)}\Theta_k + 2\sum_{k=1}^{N+4} F_{Nk}^{(1)}\Theta_k\right\}\right) = 0.$ |
| | Simply supported | $(1): W_N = 0,$ $(2),(3): \{N_{rr}, M_{rr}\} = 0 \Rightarrow \{\overline{A}, \overline{B}\}\left(\sum_{k=1}^{N+4} E_{Nk}^{(1)}\Psi_k + \nu U_N - L_c^2\left\{\sum_{k=1}^{N+4} E_{Nk}^{(3)}\Psi_k + \sum_{k=1}^{N+4} E_{Nk}^{(2)}\Psi_k - 2\sum_{k=1}^{N+4} E_{Nk}^{(2)}\Psi_k + 2U_i\right\}\right)$ $- \{\overline{B}, \overline{D}\}\left(\sum_{k=1}^{N+4} F_{Nk}^{(2)}\Theta_k + \nu\sum_{k=1}^{N+4} F_{Nk}^{(1)}\Theta_k - L_c^2\left\{\sum_{k=1}^{N+4} F_{Nk}^{(4)}\Theta_k + \sum_{k=1}^{N+4} F_{Nk}^{(3)}\Theta_k - 2\sum_{k=1}^{N+4} F_{Nk}^{(2)}\Theta_k + 2\sum_{k=1}^{N+4} F_{Nk}^{(1)}\Theta_k\right\}\right) = 0,$ |
| | Free | $(1): Q_r = 0 \Rightarrow \overline{B}\left\{\left(\sum_{k=1}^{N+4} E_{Nk}^{(2)}\Psi_k + \sum_{k=1}^{N+4} E_{Nk}^{(1)}\Psi_k - U_i\right) - L_c^2\left(\sum_{k=1}^{N+4} E_{Nk}^{(4)}\Psi_k + 2\sum_{k=1}^{N+4} E_{Nk}^{(3)}\Psi_k - 3\sum_{k=1}^{N+4} E_{Nk}^{(2)}\Psi_k + 3\sum_{k=1}^{N+4} E_{Nk}^{(1)}\Psi_k - 3U_i\right)\right\}$ $- \overline{D}\left\{\left(\sum_{k=1}^{N+4} F_{Nk}^{(3)}\Theta_k + \sum_{k=1}^{N+4} F_{Nk}^{(2)}\Theta_k - \sum_{k=1}^{N+4} F_{Nk}^{(1)}\Theta_k\right) - L_c^2\left(\sum_{k=1}^{N+4} F_{Nk}^{(5)}\Theta_k + 2\sum_{k=1}^{N+4} F_{Nk}^{(4)}\Theta_k - 3\sum_{k=1}^{N+4} F_{Nk}^{(3)}\Theta_k + 3\sum_{k=1}^{N+4} F_{Nk}^{(2)}\Theta_k - 3\sum_{k=1}^{N+4} F_{Nk}^{(1)}\Theta_k\right)\right\} = 0.$ $(2),(3): \{N_{rr}, M_{rr}\} = 0 \Rightarrow \{\overline{A}, \overline{B}\}\left(\sum_{k=1}^{N+4} E_{Nk}^{(1)}\Psi_k + \nu U_N - L_c^2\left\{\sum_{k=1}^{N+4} E_{Nk}^{(3)}\Psi_k + \sum_{k=1}^{N+4} E_{Nk}^{(2)}\Psi_k - 2\sum_{k=1}^{N+4} E_{Nk}^{(2)}\Psi_k + 2U_i\right\}\right)$ $- \{\overline{B}, \overline{D}\}\left(\sum_{k=1}^{N+4} F_{Nk}^{(2)}\Theta_k + \nu\sum_{k=1}^{N+4} F_{Nk}^{(1)}\Theta_k - L_c^2\left\{\sum_{k=1}^{N+4} F_{Nk}^{(4)}\Theta_k + \sum_{k=1}^{N+4} F_{Nk}^{(3)}\Theta_k - 2\sum_{k=1}^{N+4} F_{Nk}^{(2)}\Theta_k + 2\sum_{k=1}^{N+4} F_{Nk}^{(1)}\Theta_k\right\}\right) = 0,$ |

### 3.3. Solutions of the discretized equations of motion based on the SDM and SGT

Rearranging Eqs. (36-a,b, and c) and Table 4 (related to SDM) or Eqs. (37)-(38) and Table 5 (related to SGT), their assembled form can be presented in a similar form as shown in Refs. [66, 67] as follows:

$$\begin{bmatrix}[S_{bb}] & [S_{bd}]\\ [S_{db}] & [S_{dd}]\end{bmatrix}\begin{Bmatrix}\{U_b\}\\ \{U_d\}\end{Bmatrix} - \Omega_n^2\begin{bmatrix}[0] & [0]\\ [Q_{db}] & [Q_{dd}]\end{bmatrix}\begin{Bmatrix}\{U_b\}\\ \{U_d\}\end{Bmatrix} = \begin{Bmatrix}\{0\}\\ \{0\}\end{Bmatrix} \tag{39}$$

where,

$$\begin{aligned}\{U_b\} &= \{U_1, U_2, U_3, U_4, U_5, U_{2N+2}, U_{2N+3}, U_{2N+4}, U_{2N+5}, U_{2N+6}\}\\ &= \{W_1^{(2)}, U_1^{(1)}, W_1^{(1)}, U_1, W_1, U_N, W_N, U_N^{(1)}, W_N^{(1)}, W_N^{(2)}\}\end{aligned} \tag{40-a}$$

$$\{U_d\} = \{U_6, U_7, \ldots, U_{2N}, U_{2N+1}\} = \{U_2, W_2, U_3, W_3, \ldots, U_{N-2}, W_{N-2}, U_{N-1}, W_{N-1}\} \tag{40-b}$$

Applying the matrix sub-structuring method, Eq. (39) can be written into the following generalized eigenvalue equation:

$$\left([S]-\Omega_n^2[Q]\right)\{U_d\}=\{0\} \tag{41}$$

where the matrices **S** and **Q** are defined as:

$$[S]=[S_{dd}]-[S_{db}][S_{bb}]^{-1}[S_{bd}] \quad , \quad [Q]=[Q_{dd}]-[Q_{db}][S_{bb}]^{-1}[S_{bd}] \tag{42}$$

The non-dimensional frequencies of the nano-plate, $\Omega_n$, can be obtained by solving Eq. (41).

## 4. Validation of the Solution Procedure and Discussion of Results

### 4.1. Validation of the solution procedure

Since there are no pre-published results in the literature for the vibrational behavior of the FGM circular nano-plate based on the integral form of the SDM, then, the obtained results were compared with the vibrational behavior of a regular circular nano-plate in Ref. [48], based on the SGT. In this reference, the influences of the non-dimensional scale parameter $e_0a/R$ on the axisymmetric natural frequencies were evaluated using the classical plate theory and the nonlocal elasticity, for simply supported and clamped edge B. Cs, using the Adomian decomposition method. Table 5 shows a comparison between the results of the first two axisymmetric frequencies for this structure, based on the non-dimensional scale parameters of $e_0/R$=0.05, 0.10, 0.15, and 0.20. A different number of discrete grid points *N* along *r* direction was selected in the GDQR method to compare the deduced results with their counterpart values in Ref. [47]. In this case, the selected value of the Poisson's ratio was equal to 0.33. A comparison of these results confirms the accuracy of the proposed procedure in this analysis.

Additionally, Figs. 3 to 6, exhibit the convergence behavior of the first four axisymmetrical dimensionless frequencies of the circular nano-plate that are based on the present work for SDM and SGT, as the magnitude of *N* was increased. Here, the heterogeneity index *n* has been assumed to be equal to 2 while the value of Poisson's ratio *ν* was assumed to be 0.33. As observed, The GDQR method is well applicable to the vibrational analysis of this structure, with a fast convergence in both models, rate as *N* approaches 6 for the first mode and 10 for the second, third, and fourth modes, regardless of the type of boundary conditions imposed on the problem.

### 4.2. Discussion of results

According to the equations of motion deduced based on the nonlocal SDM and SGT, there are a few parameters that influence the vibrational behavior of the nano-plate. These parameters can be grouped as the material and geometry-related factors; namely the size parameter $L_c$, heterogeneity index *n*, and the boundary conditions. To investigate the effects of size parameter and boundary conditions on the vibrational behavior of the nanoplate, different values of frequency ratios ($R_i=\Omega_{i,\ nonlocal}/\Omega_{i,\ local}$), were plotted versus $L_{c,}$ as shown in Figs. 7 to 10, for the first four axisymmetric modes. This ratio designates the ratio of the axisymmetrical natural frequency obtained from the local model to its counterpart value obtained from the SDM/SGT, for clamped, knife, simply supported, and free edge boundary conditions. These results are based on the values of 0.33 and 10 selected for the Poisson's ratio, and the number of plate divisions in the radial direction, in the GDQR procedure, respectively. additionally, to investigate the effect of heterogeneity index *n*, the first four axisymmetrical frequencies were plotted versus the heterogeneity indices *n*, in Fig. 11 to 14. These figures are generated based on the size parameters of $L_c$=0.05 and 0.2.

**Table 6.** Comparison of the first two dimensionless natural frequencies of the circular nano-plate obtained from Ref.[48] and GDQR procedure for the non-dimensional scale parameter of $e_0/R$ and different grid points in the radial direction.

| B. Cs | Mode number | Results | | $\Omega_n=R^2\sqrt{I_0/D}\omega_n$ | | | |
|---|---|---|---|---|---|---|---|
| | | | | $e_0/R$ =0.05 | $e_0/R$ =0.10 | $e_0/R$ =0.15 | $e_0/R$ =0.20 |
| Clamped | *n*=1 | GDQR | N=4 | 10.1303 | 9.8805 | 9.5015 | 9.0361 |
| | | | N=6 | 10.1289 | 9.8793 | 9.5005 | 9.0354 |
| | | | N=8 | 10.1285 | 9.8789 | 9.5003 | 9.0352 |
| | | | N=10 | 10.1285 | 9.8789 | 9.5003 | 9.0352 |
| | | Ref.[48] | | 10.1288 | 9.8788 | 9.5003 | 9.0352 |
| | *n*=2 | GDQR | N=4 | 39.8771 | 38.0346 | 33.8556 | 29.2315 |
| | | | N=6 | 39.8112 | 38.0125 | 33.8517 | 29.1947 |
| | | | N=8 | 39.7711 | 38.0046 | 33.8496 | 29.1926 |
| | | | N=10 | 39.7711 | 38.0047 | 33.8496 | 29.1926 |
| | | Ref.[48] | | 39.7711 | 38.0047 | 33.8497 | 29.1927 |
| Simply supported | *n*=1 | GDQR | N=4 | 4.9234 | 4.8011 | 4.81223 | 4.6546 |
| | | | N=6 | 4.9212 | 4.7995 | 4.6921 | 4.5657 |
| | | | N=8 | 4.9001 | 4.7983 | 4.6412 | 4.4456 |
| | | | N=10 | 4.9001 | 4.7983 | 4.6412 | 4.4456 |
| | | Ref.[48] | | 4.9000 | 4.7982 | 4.6412 | 4.4458 |
| | *n*=2 | GDQR | N=4 | 28.9877 | 26.3366 | 23.2212 | 20.1991 |
| | | | N=6 | 28.9215 | 26.2904 | 23.1555 | 20.1887 |
| | | | N=8 | 28.8796 | 26.2561 | 23.1262 | 20.1754 |
| | | | N=10 | 28.8796 | 26.2561 | 23.1262 | 20.1754 |
| | | Ref.[48] | | 28.8795 | 26.2564 | 23.1263 | 20.1755 |

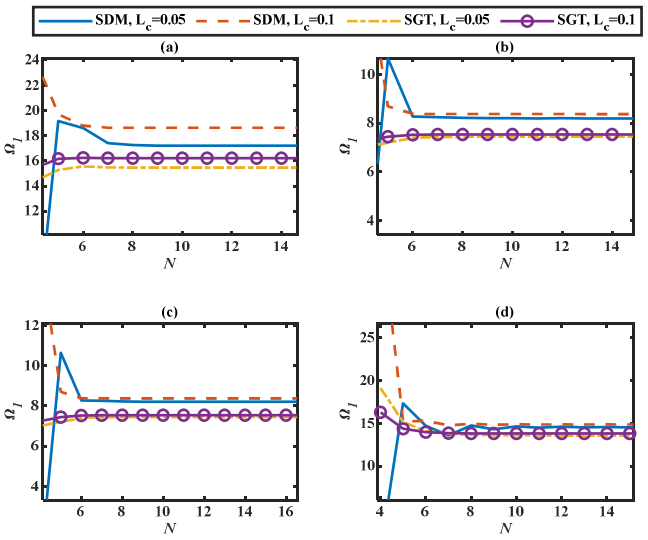


**Fig. 3.** Evaluating the convergence rate of the first axisymmetrical dimensionless frequency in the nano-plate according to the SDM and SGT, based on the two size parameters $L_c$=0.05, and 0.1, for (a) clamped (b) knife, (c) simply supported, and (d) free edge boundary conditions; the FGM heterogeneity index is $n$=2.

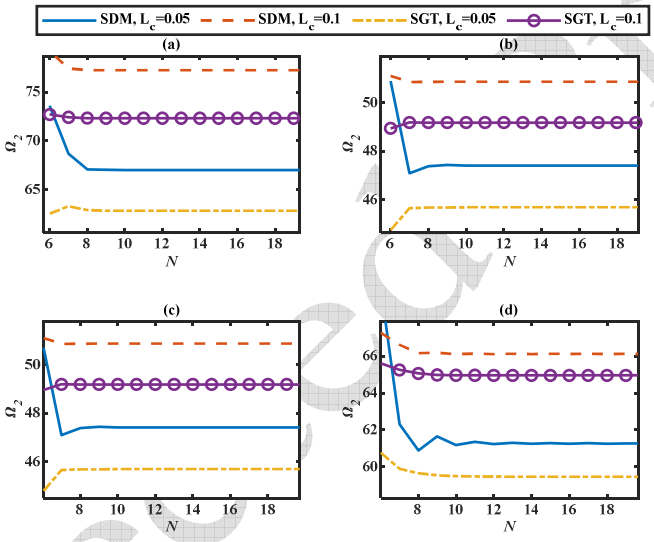


**Fig. 4.** Evaluating the convergence rate of the second axisymmetrical dimensionless frequency in the nano-plate according to the SDM and SGT, based on the two size parameters $L_c$=0.05, and 0.1, for (a) clamped (b) knife, (c) simply supported, and (d) free edge boundary conditions; the FGM heterogeneity index is $n$=2.

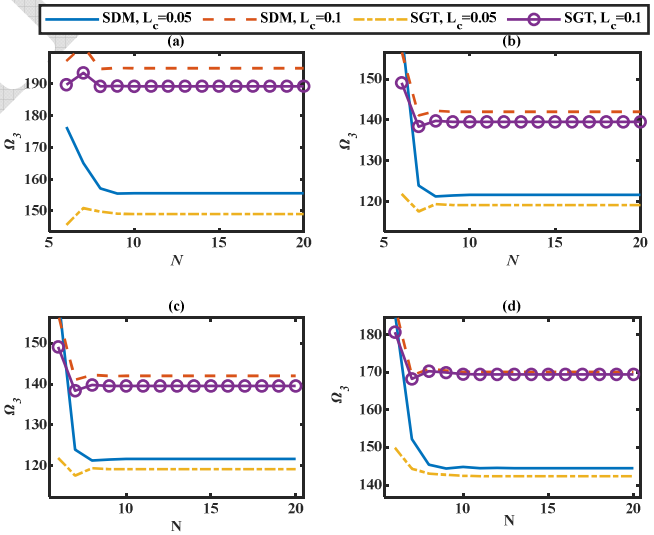


**Fig. 5.** Evaluating the convergence rate of the third axisymmetrical dimensionless frequency in the nano-plate according to the SDM and SGT, based on the two size parameters $L_c$=0.05, and 0.1, for (a) clamped (b) knife, (c) simply supported, and (d) free edge boundary conditions; the FGM heterogeneity index is $n$=2.

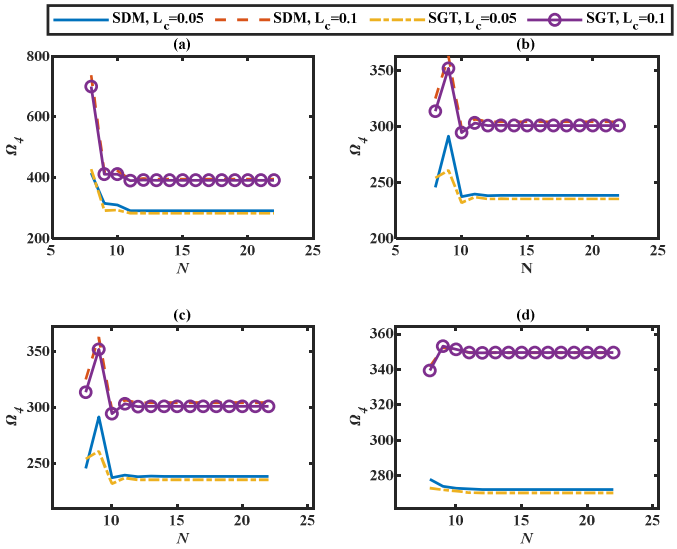


**Fig. 6.** Evaluating the convergence rate of the fourth axisymmetrical dimensionless frequency in the nano-plate according to the SDM and SGT, based on the two size parameters $L_c$=0.05, and 0.1, for (a) clamped (b) knife, (c) simply supported, and (d) free edge boundary conditions; the FGM heterogeneity index is $n$=2.

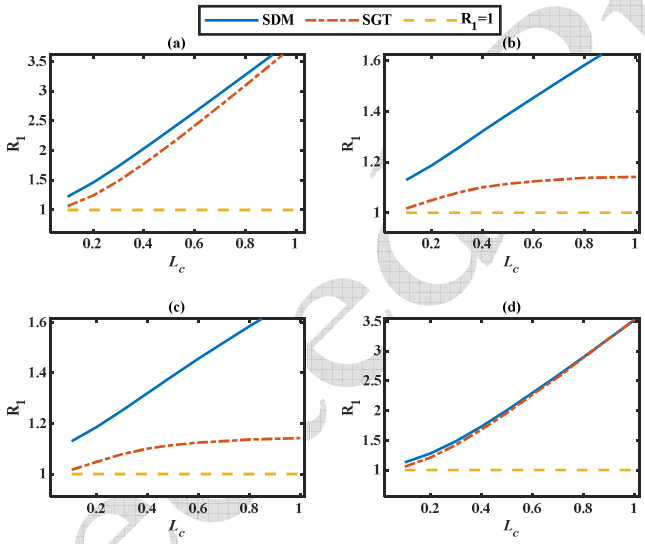


**Fig. 7.** The effect of size parameter on the first axisymmetric mode of the circular nano-plate with (a) clamped, (b) knife-edge, (c) simply supported, and (d) free edge boundary conditions and FGM heterogeneity index of $n$=1.

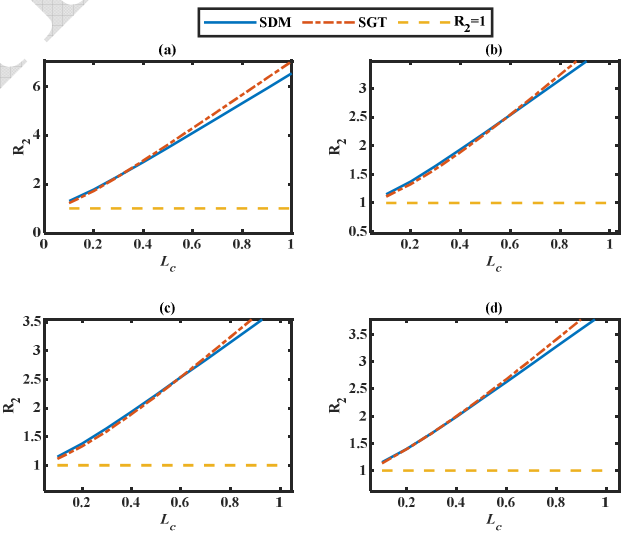


**Fig. 8.** The effect of size parameter on the second axisymmetric mode of the circular nano-plate with (a) clamped, (b) knife-edge, (c) simply supported, and (d) free edge boundary conditions and FGM heterogeneity index of $n$=1.

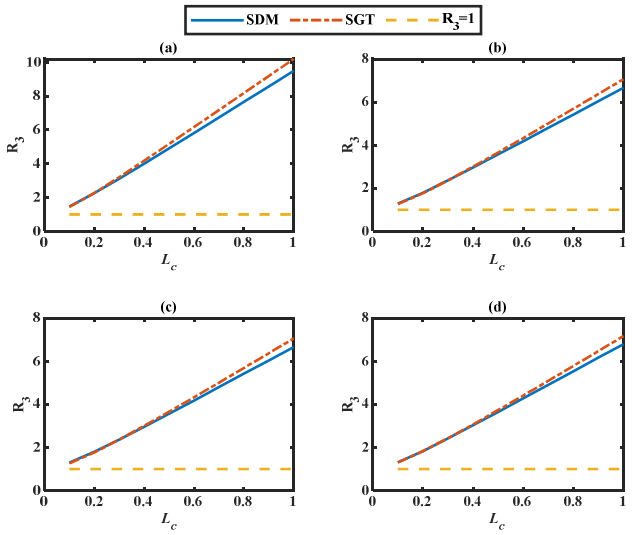


**Fig. 9.** The effect of size parameter on the third axisymmetric mode of the circular nano-plate with (a) clamped, (b) knife-edge, (c) simply, and (d) free edge boundary conditions and FGM heterogeneity index of $n$=1.

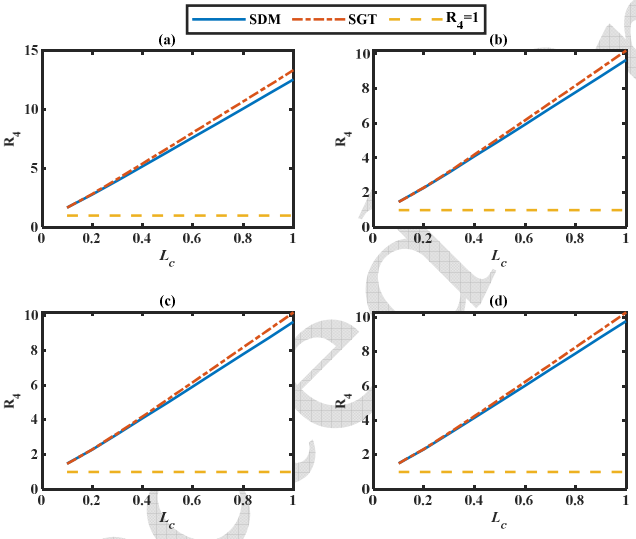


**Fig. 10.** The effect of size parameter on the four axisymmetric mode of the circular nano-plate with (a) clamped, (b) knife-edge, (c) simply, and (d) free edge boundary conditions and FGM heterogeneity index of $n$=1.

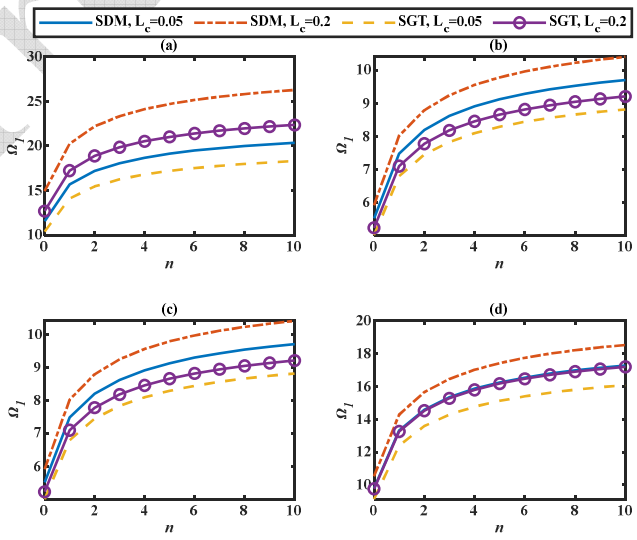


**Fig. 11.** The effect of heterogeneity index $n$, nonlocal models, and boundary conditions on the first axisymmetric mode of the circular nano-plate with (a) clamped, (b) knife-edge, (c) simply supported, and (d) free edge boundary conditions for different values of size parameters.

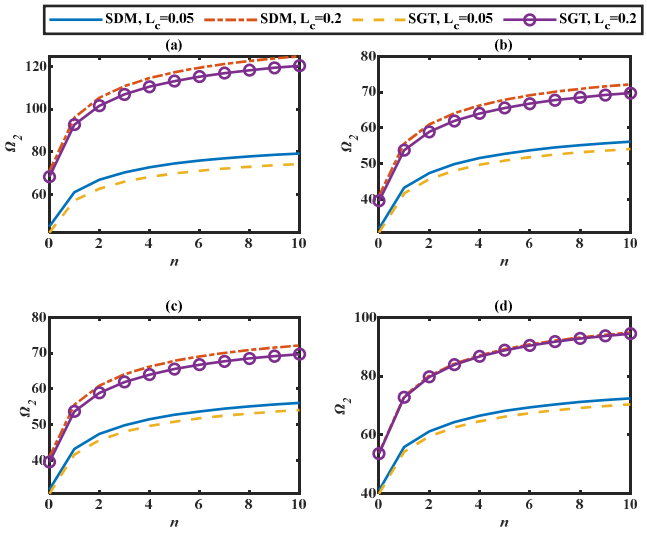


**Fig. 12.** The effect of heterogeneity index *n*, nonlocal models, and boundary conditions on the second axisymmetric mode of the circular nanoplate with (a) clamped, (b) knife-edge, (c) simply supported, and (d) free edge boundary conditions for different values of size parameters.

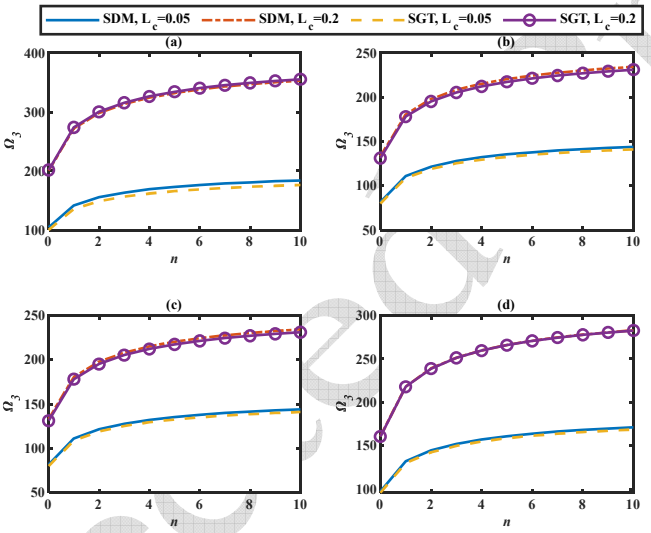


**Fig. 13.** The effect of heterogeneity index *n*, nonlocal models, and boundary conditions on the third axisymmetric mode of the circular nanoplate with (a) clamped, (b) knife-edge, (c) simply supported, and (d) free edge boundary conditions for different values of size parameters.

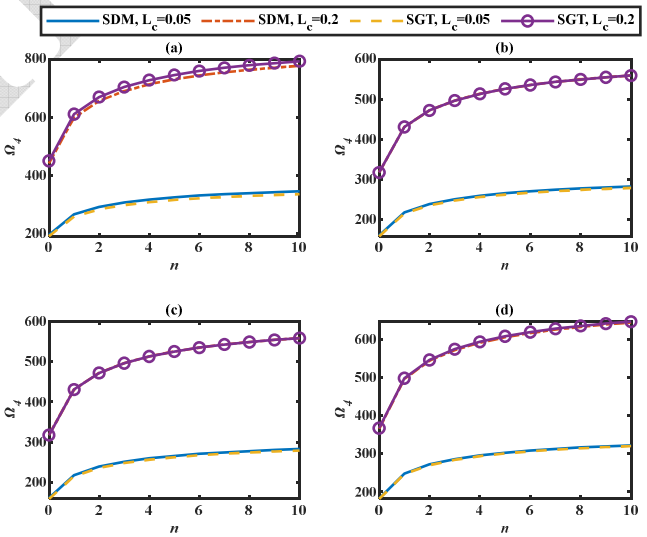


**Fig. 14.** The effect of heterogeneity index *n*, nonlocal models, and boundary conditions on the fourth axisymmetric mode of the circular nanoplate with (a) clamped, (b) knife-edge, (c) simply supported, and (d) free edge boundary conditions for different values of size parameters.

#### 4.2.1. *The effect of size parameter $L_c$ and boundary conditions on the vibrational behavior*

As shown in Figs. 7 to 10, with an increase in size parameter $L_c$, the frequency ratio for both nonlocal SDM and SGT increases for all types of boundary conditions and vibrational modes. This indicates that the use of both nonlocal models leads to the stiffening behavior for the nanoplate, and thus the value of natural frequency increases compared with the classical local model.

Figures 7(b, and c) indicate that for the knife and simply supported edge boundary conditions, the SDM model predicts a higher rate of increase in values of frequency ratio in the first mode of vibration while showing more sensitivity to all values of $L_c$; and hence, it appears to be a more reliable model for the prediction of the vibrational behavior of the nano-plate. However, similar behaviors were observed for clamped and free edge boundary conditions, as shown in Figs. 7(a, and d).

According to Figure 8, both the SDM and SGT appear to be good models for the prediction of the second mode of vibrational behavior of the nano-plate for all types of considered boundary conditions. However, the SDM model shows a minute stiffer behavior in the vibrational behavior of the nanoplate, compared with the SGT model, for values of $L_c$ less than 0.4 for the clamped edge, 0.6 for the knife as well as the simply supported edges, and 0.5 for the free edge boundary condition. Additionally, as shown in Figs. 9 and 10, both the SDM and SGT appear to be good models for the prediction of the third and the fourth vibrational mode, for all types of boundary conditions. Based on these figures, the difference between the two models appears to be very small.

#### 4.2.2. *The effect of heterogeneity index n and boundary conditions*

The effect of heterogeneity index $n$ on the first four axisymmetrical modes of vibration for the circular nano-plate is shown in Figs. 11 to 14. As shown, increasing the material index $n$ increases the value of natural frequency obtained by SDM and SGT. However, in this structure, for the knife and simply supported edges, the two aforementioned nonlocal models predict almost the same value for $\Omega_i$, as $n$ is increased. Moreover, for the size parameters $L_c$=0.05 and 0.2, although the SDT predicts higher values of $\Omega_i$ for any specific value of $n$, yet, all models show similar sensitivities to the index number $n$ as its value is altered.

## 5. Conclusions

The vibrational behavior of a circular nano-plate was analyzed using the nonlocal SDM and SGT. Different possible boundary conditions were imposed on the nano-plate to examine their effect on the vibrational frequency. To get the solution, the deduced equilibrium equations of motion were solved using the general differential quadrature rule (GDQR). Examination of the obtained results revealed the influence of various parameters such as size-effect parameter $L_c$, material heterogeneity index $n$, and their corresponding boundary conditions on the first four symmetrical frequencies.

According to the findings, the stress-driven model appears to be a good model for the prediction of vibrational behavior of the nano-plate due to its simplicity in;

- Derivation of the required equations of motion;
- Adaptively of the equations to model the nano-plate based on different types of boundary conditions imposed on the edges;
- Its versatility to the application of GDQR numerical solution;

Additionally, it was found that;

- In all modes of vibration, the increase in size parameter $L_c$, increases the frequency ratio in both SDM and SGT nonlocal models, for all types of boundary conditions. This is interpreted as the use of both nonlocal models leads to stiffening behavior in this structure, and thus, the value of natural frequency increases compared with the classical local model.
- For the knife and simply supported boundary conditions, the SDM model predicts a higher rate of increase in values of frequency ratio in the first mode of vibration, while showing more sensitivity to all values of $L_c$; and hence, it appears to be a more reliable model for the prediction of the first mode of vibrational behavior of the nano-plate.
- SDM and SGT appear to be good models for the prediction of the second, third and fourth modes of vibration, for all postulated types of boundary conditions.
- In the second mode of vibration, the SDM shows a minute stiffer behavior in the vibrational behavior of the nanoplate, compared with the SGT model, for values of $L_c$ less than 0.4 for the clamped edge, 0.6 for the knife as well as the simply supported edges, and 0.5 for the free edge boundary condition. A similar trend appears to exists for the third mode, while in the fourth mode, this behavior is observed for the values of $L_c$ less than 0.4, for all types of boundary conditions.

## Acknowledgment

This work has been supported by Shahid Chamran University of Ahvaz under grant No. SCU.EM99.561.

## Author Contributions

All authors made a substantial, direct and intellectual contribution to this work. The manuscript was written through the contribution of all authors. All authors discussed the results, reviewed and approved the final version of the manuscript.

## Conflict of Interest

The authors declare no potential conflicts of interest with respect to the research, authorship, and publication of this article.

## Funding

This work was performed at Shahid Chamran University of Ahvaz under the grant No. SCU.EM99.561.

## Data Availability Statements

The datasets generated and/or analyzed during the current study are available from the corresponding author on reasonable request.

## References


1. Eringen, A.C. and D.J.I.j.o.e.s. Edelen, On nonlocal elasticity. 1972. 10(3): p. 233-248.
2. Aifantis, E.C., Gradient deformation models at nano, micro, and macro scales. 1999.
3. Aifantis, E.C., Strain gradient interpretation of size effects, in Fracture Scaling. 1999, Springer. p. 299-314.
4. Gutkin, M.Y. and E.J.S.M. Aifantis, Edge dislocation in gradient elasticity. 1997. 36(1).
5. Apuzzo, A., et al., Novel local/nonlocal formulation of the stress-driven model through closed form solution for higher vibrations modes. Composite Structures, 2020. 252: p. 112688.
6. Sedighi, H.M. and M.J.P.S. Malikan, Stress-driven nonlocal elasticity for nonlinear vibration characteristics of carbon/boron-nitride hetero-nanotube subject to magneto-thermal environment. 2020. 95(5): p. 055218.
7. Yang, X., S. Sahmani, and B. Safaei, Postbuckling analysis of hydrostatic pressurized FGM microsized shells including strain gradient and stress-driven nonlocal effects. Engineering with Computers, 2020.
8. Shariati, M., et al., On the calibration of size parameters related to non-classical continuum theories using molecular dynamics simulations. International Journal of Engineering Science, 2021. 168: p. 103544.
9. Shishesaz, M., M. Shariati, and M. Hosseini, Size effect analysis on Vibrational response of Functionally Graded annular nano plate based on Nonlocal stress-driven method. International Journal of Structural Stability and Dynamics, 2021, In press.
10. Li, L., R. Lin, and Y. Hu, Cross-section effect on mechanics of nonlocal beams. Archive of Applied Mechanics, 2021. 91(4): p. 1541-1556.
11. Li, L., R. Lin, and T.Y. Ng, Contribution of nonlocality to surface elasticity. International Journal of Engineering Science, 2020. 152: p. 103311.
12. Jiang, P., H. Qing, and C. Gao, Theoretical analysis on elastic buckling of nanobeams based on stress-driven nonlocal integral model. Applied Mathematics and Mechanics, 2020. 41(2): p. 207-232.
13. Barretta, R., et al., Buckling loads of nano-beams in stress-driven nonlocal elasticity. Mechanics of Advanced Materials and Structures, 2020. 27(11): p. 869-875.
14. Luciano, R., et al., Free flexural vibrations of nanobeams with non-classical boundary conditions using stress-driven nonlocal model. Mechanics Research Communications, 2020. 107: p. 103536.
15. Pinnola, F.P., et al., Random vibrations of stress-driven nonlocal beams with external damping. Meccanica, 2020.
16. Luciano, R., et al., Variational approaches for bending and buckling of non-local stress-driven Timoshenko nano-beams for smart materials. Mechanics Research Communications, 2020. 103: p. 103470.
17. He, Y., H. Qing, and C.-F. Gao, Theoretical Analysis of Free Vibration of Microbeams under Different Boundary Conditions Using Stress-Driven Nonlocal Integral Model. 2020. 20(03): p. 2050040.
18. Roghani, M. and H. Rouhi, Nonlinear stress-driven nonlocal formulation of Timoshenko beams made of FGMs. Continuum Mechanics and Thermodynamics, 2020.
19. Romano, G. and R. Barretta, Nonlocal elasticity in nanobeams: the stress-driven integral model. International Journal of Engineering Science, 2017. 115: p. 14-27.
20. Apuzzo, A., et al., Free vibrations of Bernoulli-Euler nano-beams by the stress-driven nonlocal integral model. Composites Part B: Engineering, 2017. 123: p. 105-111.
21. Maneshi, M.A., E. Ghavanloo, and S.A. Fazelzadeh, Well-posed nonlocal elasticity model for finite domains and its application to the mechanical behavior of nanorods. Acta Mechanica, 2020. 231(10): p. 4019-4033.
22. Zhang, P. and H. Qing, Exact solutions for size-dependent bending of Timoshenko curved beams based on a modified nonlocal strain gradient model. Acta Mechanica, 2020.
23. Malikan, M., V.A. Eremeyev, and H.M. Sedighi, Buckling analysis of a non-concentric double-walled carbon nanotube. Acta Mechanica, 2020.
24. Espo, M., M.H. Abolbashari, and S.M. Hosseini, Band structure analysis of wave propagation in piezoelectric nano-metamaterials as periodic nano-beams considering the small scale and surface effects. Acta Mechanica, 2020. 231(7): p. 2877-2893.
25. Al-Furjan, M.S.H., M. Habibi, and H. Safarpour, Vibration Control of a Smart Shell Reinforced by Graphene Nanoplatelets. 2020. 12(06): p. 2050066.
26. Khoram, M.M., et al., Bending Analysis of Bi-Directional FGM Timoshenko Nano-Beam subjected to mechanical and magnetic forces and resting on Winkler-Pasternak foundation. 0(ja): p. null.
27. Barati, A., M.M. Adeli, and A. Hadi, Static Torsion of Bi-Directional Functionally Graded Microtube Based on the Couple Stress Theory Under Magnetic Field. 2020. 12(02): p. 2050021.
28. Xing, Y., et al., Surface Effects on Large Deflection of Nanobeams Subjected to a Follower Load. 2020. 12(06): p. 2050067.
29. Hadi, A., M.Z. Nejad, and M. Hosseini, Vibrations of three-dimensionally graded nanobeams. International Journal of Engineering Science, 2018. 128: p. 12-23.
30. Hosseini, M., et al., Stress analysis of rotating nano-disks of variable thickness made of functionally graded materials. International Journal of Engineering Science, 2016. 109: p. 29-53.
31. Hosseini, M., et al., Size-Dependent Stress Analysis of Single-Wall Carbon Nanotube Based on Strain Gradient Theory. 2017. 09(06): p. 1750087.
32. Adeli, M.M., et al., Torsional vibration of nano-cone based on nonlocal strain gradient elasticity theory. The European Physical Journal Plus, 2017. 132(9): p. 393.
33. Hosseini, M., et al., A review of size-dependent elasticity for nanostructures. 2018. 49(1): p. 197-211.
34. Shishesaz, M., et al., Analysis of functionally graded nanodisks under thermoelastic loading based on the strain gradient theory. Acta Mechanica, 2017. 228(12): p. 4141-4168.
35. Hosseini, M., M. Shishesaz, and A. Hadi, Thermoelastic analysis of rotating functionally graded micro/nanodisks of variable thickness. Thin-Walled Structures, 2019. 134: p. 508-523.
36. Mohammadi, M., et al., Primary and secondary resonance analysis of porous functionally graded nanobeam resting on a nonlinear foundation subjected to mechanical and electrical loads. European Journal of Mechanics - A/Solids, 2019. 77: p. 103793.
37. Haghshenas Gorgani, H., M. Mahdavi Adeli, and M. Hosseini, Pull-in behavior of functionally graded micro/nano-beams for MEMS and NEMS switches. Microsystem Technologies, 2019. 25(8): p. 3165-3173.
38. Shishesaz, M. and M. Hosseini, Mechanical Behavior of Functionally Graded Nano-Cylinders Under Radial Pressure Based on Strain Gradient Theory. Journal of Mechanics, 2019. 35(4): p. 441-454.
39. Mousavi Khoram, M., M. Hosseini, and M. Shishesaz, A concise review of nano-plates. 2019. 50(2): p. 420-429.
40. Hadi, A., et al., Buckling analysis of FGM Euler-Bernoulli nano-beams with 3D-varying properties based on consistent couple-stress theory. Steel and Composite Structures, 2018. 26(6): p. 663-672.
41. Najafzadeh, M., et al., Torsional vibration of the porous nanotube with an arbitrary cross-section based on couple stress theory under magnetic field. Mechanics Based Design of Structures and Machines, 2020: p. 1-15.
42. Karami, B., et al., On the resonance of functionally graded nanoplates using bi-Helmholtz nonlocal strain gradient theory. International Journal of Engineering Science, 2019. 144: p. 103143.
43. Bisheh, H. and Ö. Civalek, Vibration of smart laminated carbon nanotube-reinforced composite cylindrical panels on elastic foundations in hygrothermal environments. Thin-Walled Structures, 2020. 155: p. 106945.
44. Salehipour, H., et al., Static deflection and free vibration analysis of functionally graded and porous cylindrical micro/nano shells based on the three-dimensional elasticity and modified couple stress theories. Mechanics Based Design of Structures and Machines, 2020: p. 1-22.
45. Shishesaz, M., et al., Nonlinear Vibration Analysis of Nano-Disks Based on Nonlocal Elasticity Theory Using Homotopy Perturbation Method. 2019. 11(02): p. 1950011.
46. Zarei, M., et al., Buckling and vibration analysis of tapered circular nano plate. Journal of Applied and Computational Mechanics, 2018. 4(1): p. 40-54.
47. Barretta, R., S.A. Faghidian, and F.M. De Sciarra, Stress-driven nonlocal integral elasticity for axisymmetric nano-plates. International Journal of Engineering Science, 2019. 136: p. 38-52.
48. Shishesaz, M., M. Shariati, and A. Yaghootian, Nonlocal Elasticity Effect on Linear Vibration of Nano-circular Plate Using Adomian Decomposition Method. Journal of Applied and Computational Mechanics, 2020. 6(1): p. 63-76.

49. Shariati, M., et al., Nonlinear Vibration Analysis of circular plate Based on Nonlocal Elasticity Theory Using Variational Iteration Method. Journal of Applied and Computational Mechanics, 2021, In press.
50. Li, A., et al., Nonlinear axisymmetric bending analysis of strain gradient thin circular plate. Applied Mathematical Modelling, 2021. 89: p. 363-380.
51. Al-Furjan, M., et al., Vibrational characteristics of a higher-order laminated composite viscoelastic annular microplate via modified couple stress theory. Composite Structures, 2021. 257: p. 113152.
52. Li, L., L. Xiaobai, and H. Yujin, Free vibration analysis of nonlocal strain gradient beams made of functionally graded material. International Journal of Engineering Science, 2016. 102: p. 77-92.
53. Barretta, R., Analogies between Kirchhoff plates and Saint-Venant beams under flexure. Acta Mechanica, 2014. 225(7): p. 2075-2083.
54. Barretta, R., Analogies between Kirchhoff plates and Saint-Venant beams under torsion. Acta Mechanica, 2013. 224(12): p. 2955-2964.
55. Luo, Q., C. Li, and S. Li, Transverse Free Vibration of Axisymmetric Functionally Graded Circular Nanoplates with Radial Loads. Journal of Vibration Engineering & Technologies, 2021: p. 1-16.
56. Pourabdy, M., Shishesaz, Mohammad, Shahrooi, Shahram, Roknizadeh, Alireza, Analysis of Axisymmetric Vibration of Functionally-Graded Circular Nano-Plate Based on the Integral Form of the Strain Gradient Model. Journal of Applied and Computational Mechanics, 2021.
57. Barretta, R., et al., Free vibrations of FG elastic Timoshenko nano-beams by strain gradient and stress-driven nonlocal models. Composites Part B: Engineering, 2018. 154: p. 20-32.
58. Zhang, P. and H. Qing, Buckling analysis of curved sandwich microbeams made of functionally graded materials via the stress-driven nonlocal integral model. Mechanics of Advanced Materials and Structures, 2020: p. 1-18.
59. Penna, R., et al., Nonlinear free vibrations analysis of geometrically imperfect FG nano-beams based on stress-driven nonlocal elasticity with initial pretension force. Composite Structures, 2021. 255: p. 112856.
60. Timoshenko, S.P. and S. Woinowsky-Krieger, Theory of plates and shells. 1959: McGraw-hill.
61. Barretta, R., S.A. Faghidian, and F. Marotti de Sciarra, Stress-driven nonlocal integral elasticity for axisymmetric nano-plates. International Journal of Engineering Science, 2019. 136: p. 38-52.
62. Zhao, J. and D. Pedroso, Strain gradient theory in orthogonal curvilinear coordinates. International Journal of Solids and Structures, 2008. 45(11-12): p. 3507-3520.
63. Wu, T.Y. and G.R. Liu, Application of generalized differential quadrature rule to sixth-order differential equations. 2000. 16(11): p. 777-784.
64. Shu, C. and B.E. Richards, Application of generalized differential quadrature to solve two-dimensional incompressible Navier-Stokes equations. 1992. 15(7): p. 791-798.
65. Quan, J.R. and C.T. Chang, New insights in solving distributed system equations by the quadrature method—I. Analysis. Computers & Chemical Engineering, 1989. 13(7): p. 779-788.
66. Kang, K., C.W. Bert, and A.G. Striz, Vibration analysis of shear deformable circular arches by the differential quadrature method. Journal of Sound and Vibration, 1995. 183(2): p. 353-360.
67. Wu, T.Y. and G.R. Liu, The generalized differential quadrature rule for fourth-order differential equations. 2001. 50(8): p. 1907-1929.


## ORCID iD


Mojtaba Shariati https://orcid.org/0000-0002-7032-548X
Mohammad Shishehsaz https://orcid.org/0000-0002-1892-1946
Reza Mosalmani https://orcid.org/0000-0002-8036-9638
S. Alireza S. Roknizadeh https://orcid.org/0000-0002-6731-7956





**How to cite this article:** Shariati M., Shishehsaz M., Mosalmani R., Roknizadeh S.A.S. Size Effect on the Axisymmetric Vibrational Response of Functionally Graded Circular Nano-Plate Based on the Nonlocal Stress-Driven Method, *J. Appl. Comput. Mech.*, xx(x), 2021, 1–19. https://doi.org/10.22055/JACM.2021.38131.3159